Hierarchical Self-Organization of Perylene Bisimide–Melamine Assemblies to Fluorescent Mesoscopic Superstructures

Frank Würthner,*[a] Christoph Thalacker,[a] Armin Sautter,[a] Wolfgang Schärtl,[b] Wolfram Ibach,[c] and Olaf Hollricher[c]

Abstract: A series of three perylene tetracarboxylic acid bisimide dyes **3a–c** bearing phenoxy substituents at the four bay positions of the perylene core were synthesized and their complexation behavior to complementary ditopic dialkyl melamines **8a–c** was investigated. Binding constants and Gibbs binding energies for the hydrogen bonds between the imide and the complementary melamine moiety have been determined in several solvents by NMR and UV/Vis titration experiments with monotopic model compounds **5** and **9**. The effects of the solvent polarity and specific solvent–solute interactions on the degree of polymerization of $(\mathbf{3}\cdot\mathbf{8})_n$ are discussed, and a general formula to estimate the chain length of $[AA-BB]_n$ nylon-type supramolecular polymers is derived. In addition to the formation of a hydrogen-bonded supramolecular chain, $\pi-\pi$ interactions were observed for perylene bisimide–melamine assemblies **3b·8b** and **3b·8c** in aliphatic solvents. The orthogonal nature of hydrogen bonding and $\pi-\pi$ interactions leads to three-dimensional growth yielding large-sized aggregates already in dilute solution. On suitable substrates, densely intertwined networks of nano- to mesoscopic strands are formed which have been investigated by electron microscopy, confocal fluorescence microscopy and optical polarization microscopy. The high fluorescence and excellent photostability of these superstructures is promising for future studies on energy migration and artificial light harvesting at the nano- and mesoscopic length scale.

Keywords: dyes · fluorescence · nanostructures · noncovalent interactions · supramolecular chemistry

Introduction

In nature, complex functional units are organized hierarchically over several length scales by multiple noncovalent interactions.[1] As an especially intriguing example, the structure of the light harvesting complex of purple bacteria has recently been elucidated, in which hundreds of chlorophyll and carotene molecules are organized within highly symmetric cyclic structures.[2] Based on their optimized arrangement in space these "antennae" are able to take up a maximum of solar energy and transfer it to the reaction center where charge separation takes place. In contrast to a number of noncovalently assembled model systems containing porphyrin and phthalocyanine dyes,[3] the organization of the chlorophyll chromophores within this light harvesting system is only marginally based on $\pi-\pi$ interactions, but mainly on the interaction of the dyes with the protein matrix. In simplified terms, these protein units play the part of a "molecular glue" to ensure 1) the optimal positioning of the chromophores in space and 2) the control of their interactions for maximization of the vectorial transport of excitation energy from the outer pigments to the central unit which contains the reaction center of photosynthesis.

This fascinating architecture and its unique functionality motivated us to conceive defined functional nano- and mesoscopic structures from complementary molecular building blocks with the final goal of artificial light harvesting. In order to ensure a most rational and variable design, one of the building blocks should bear the functional properties, whereas the other should provide the scaffold similar to the protein in the light harvesting complex. A promising supramolecular synthon for this purpose is given by the highly directional triple hydrogen bonding of bisimides with ditopic melamines which has been successfully used to design a number of supramolecular assemblies.[4] The ditopic nature of both binding partners should lead to an association polymer in form of a linearly or helically grown tape structure. Additional

[a] Dr. F. Würthner, C. Thalacker, A. Sautter
Abteilung Organische Chemie II, Universität Ulm
Albert-Einstein-Allee 11, 89081 Ulm (Germany)
Fax: (+49) 731-5022840
E-mail: frank.wuerthner@chemie.uni-ulm.de

[b] Dr. W. Schärtl
Institut für Physikalische Chemie
Universität Mainz, Jakob-Welder-Weg 11, 55099 Mainz (Germany)

[c] W. Ibach, Dr. O. Hollricher
Abteilung Experimentelle Physik, Universität Ulm
Albert-Einstein-Allee 11, 89081 Ulm (Germany)

  0947-6539/00/0621-3871 $ 17.50+.50/0

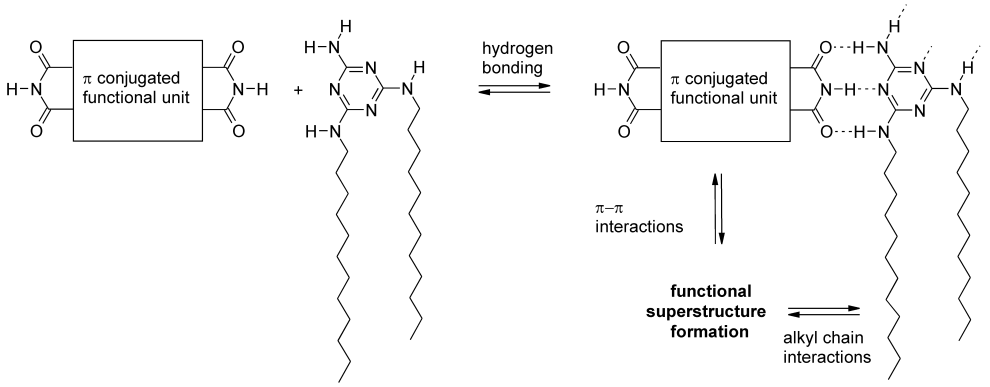

Scheme 1. Formation of functional superstructures by hierarchical self-organization involving orthogonal intermolecular interactions as given with hydrogen bonding, π–π- and alkyl chain interactions.

weaker interactions between the π surfaces of these chains might lead to a further organization process to three-dimensional structures similar to the folding of peptide chains in proteins (Scheme 1).

Tetraphenoxy substituted perylene bisimides were chosen as functional building blocks, which are known to exhibit particularly promising optical properties, that is fluorescence quantum yields of almost 100% as well as a very high photostability.[5, 6] In this paper we report the synthesis of tetraphenoxy substituted perylene tetracarboxylic acid bisimides, superstructure formation with complementary dialkyl melamines to give mesoscopic strands and the investigation of their optical properties. Our studies include careful experiments on hydrogen bonding and π–π interactions in various solvents using appropriate model compounds, the dependence of superstructure formation on the substituents at the perylene and melamine subunits, and the characterization of the solid complexes by optical spectroscopy, electron microscopy, and confocal fluorescence microscopy.

Abstract in German: *Die Synthese von drei Perylentetracarbonsäurebisimid-Farbstoffen **3a–c** mit unterschiedlichen Phenoxysubstituenten in den „Bay"-Positionen des Perylenkörpers und ihr Komplexierungsverhalten mit komplementären Dialkylmelaminen **8a–c** wird beschrieben. Mittels der monotopen Modellverbindungen **5** und **9** wurden die Bindungskonstanten und die Freien Enthalpien der Wasserstoffbrückenbindung zwischen den Imidgruppen und den Melaminen in zahlreichen Lösungsmitteln mittels NMR- und UV/Vis-spektroskopischer Titrationsexperimente bestimmt. Die dabei beobachteten spezifischen und unspezifischen Wechselwirkungen zwischen den Bindungspartnern und dem Lösungsmittel und ihr Einfluß auf den Polymerisationsgrad von $(3 \cdot 8)_n$ werden diskutiert und eine allgemeine Formel zur Abschätzung der Länge supramolekularer Polymere vom Nylon-Typ $[AA-BB]_n$ wird abgeleitet. Zusätzlich zur Ausbildung einer mittels Wasserstoffbrückenbindungen verknüpften supramolekularen Kette konnten für die Perylenbisimid–Melamin-Assoziationspolymere **3b·8b** und **3b·8c** π–π-Wechselwirkungen beobachtet werden. Durch die orthogonale Natur von Wasserstoffbrücken- und π–π-Wechselwirkungen findet ein dreidimensionaler Wachstumsprozeß zu ausgedehnten Aggregaten bereits in verdünnter Lösung statt. Nach Verdampfen dieser Lösungen auf geeigneten Oberflächen wurden dicht ineinander verwundene Netzwerke nano- und mesoskopischer Stränge erhalten, die mit elektronenmikroskopischen Methoden, konfokaler Fluoreszenzmikroskopie, sowie Polarisationsmikroskopie charakterisiert werden konnten. Die intensive Fluoreszenz und die Photostabilität von **3b·8b, c**-Überstrukturen erscheinen vielversprechend für zukünftige Experimente, mit denen gerichtete Energietransport- und Lichtsammelprozesse auf der nano- und mesoskopischen Längenskala untersucht werden sollen.*

Results and Discussion

Synthesis: Perylene tetracarboxylic acid bisimides are known as radiant colorants of outstanding lightfastness, chemical inertness, and high fluorescence quantum yields.[7] However, their use as fluorescent dyes required considerable efforts to overcome their intrinsically low solubility. Thus, Langhals introduced branched alkyl chains at the imide functionality,[8] whereas Seybold et al. and Müllen et al. developed methods to introduce solubilizing substituents in the bay region of these dyes.[5] The latter approach seemed to be promising with regard to soluble functional building blocks bearing free imide groups for hydrogen bonding. For our studies, three different phenols were used in order to study the influence of sterical contributions on solubility and superstructure formation (Scheme 2).

Our synthesis started with *n*-butyl substituted tetracarboxylic acid bisimides **1a–c** which were treated with potassium hydroxide in *tert*-butyl alcohol[8b] to give the corresponding bisanhydrides **2a–c**. Compounds **2a, b** were treated with ammonium acetate in refluxing propionic acid to yield the bisimides **3a, b**. Owing to the insufficient stability of bisanhydride **2c** under these conditions, bisimide **3c** was synthesized under milder conditions by reacting **2c** with gaseous ammonia in *N*-methyl-2-pyrrolidone (NMP) using zinc acetate as a Lewis acid catalyst.

As a high purity of the compounds is crucial for our studies on the formation of extended superstructures (vide infra), an efficient way to purify bisimide **3a** was needed, which is almost insoluble in organic solvents. For bisimide **3b**, a higher

  0947-6539/00/0621-3872 $ 17.50+.50/0 *Chem. Eur. J.* **2000**, *6*, No. 21

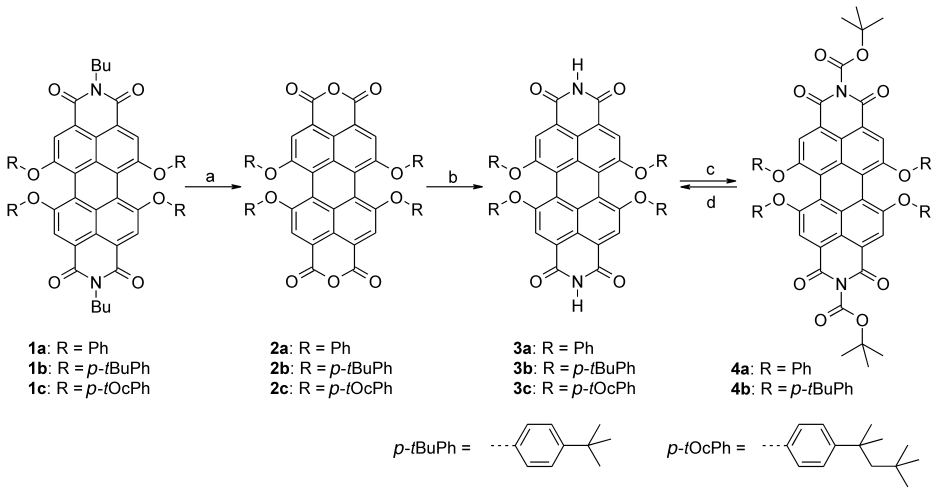

Scheme 2. Synthesis and purification of the perylene bisimides **3a–c**. a) KOH, *t*BuOH, 80 °C, 10 h, 95 %. b) **3a, b**: Ammonium acetate (100 equiv), propionic acid, 140 °C, 16 h, 60 %; **3c**: Zinc acetate, NMP, 80 °C, 8 h, 40 %. c) Boc_2O (8 equiv), DMAP, DMF, Ar, 25 °C, 5 h, 40 %. d) CF_3COOH, CH_2Cl_2, 25 °C, 4 h, 98 %.

solubility was also desirable to accomplish chromatographic purification. Following a recent method for the purification of lactam pigments,[9] the sparingly soluble crude bisimides **3a, b** were treated with di-*tert*-butyldicarbonate (Boc_2O)[10] to yield the highly soluble dyes **4a, b** which could easily be purified by chromatography. In addition to the increased solubility, the *tert*-butoxycarbonyl group (Boc),which is widely used in many fields of synthetic chemistry, has the advantage to be stable under basic conditions, but can easily be removed in acidic media or by thermal treatment without even traces of impurities. Accordingly, the pure Boc-substituted compounds were deprotected quantitatively with trifluoroacetic acid in dichloromethane to give pure bisimides **3a, b** (Scheme 2).

In order to study binding properties between perylene imides and melamines, monotopic model compounds are preferred which form defined complexes of 1:1 stoichiometry. Thus, the unsymmetrically substituted bisimide **5** was synthesized by subsequent reaction of bisanhydride **2b** with 2-ethylhexylamine in toluene and ammonia in propionic acid. Due to its excellent solubility, compound **5** could easily be separated from the symmetric by-products by column chromatography. Another model compound, the *N*,*N*′-dialkyl substituted bisimide **6**, was included in our study to estimate the contribution of $\pi-\pi$ interactions to superstructure formation (Scheme 3).

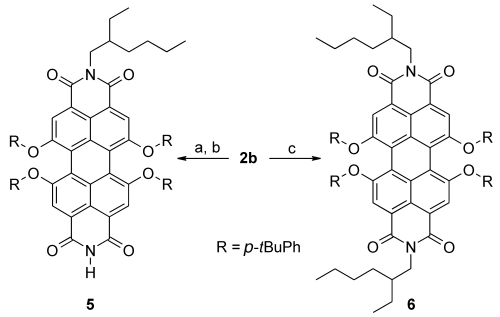

Scheme 3. Synthesis of model compounds for binding studies. a) 2-Ethylhexylamine (1 equiv), toluene, 110 °C, 20 h. b) NH_3 (200 equiv), propionic acid, 140 °C, 14 h, 26 %. c) 2-Ethylhexylamine (4 equiv), propionic acid, 140 °C, 16 h, 83 %.

The ditopic melamines **8a–c** were synthesized according to the literature,[11, 12] and the monotopic melamine receptor **9** was obtained by subsequent reaction of cyanuric chloride **7** with aqueous ammonia in acetone and di(2-ethylhexyl)amine in DMF according to Scheme 4.

Imide–melamine hydrogen bonding: Imide–melamine systems have been widely used in supramolecular chemistry, and for many different compounds binding constants have been determined mainly based on NMR titration experiments.[4] Most of these studies have been restricted to variations of the

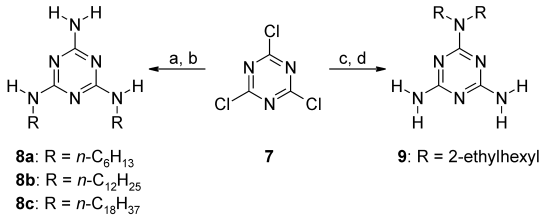

Scheme 4. Synthesis of the melamines **8a–c** and **9**. a) NH_3, dioxane/ethyleneglycol dibutylether 10:1, 0–10 °C, 50 %. b) RNH_2, dioxane, $NaHCO_3$, 100 °C, 24h, 80–90 %. c) NH_3, H_2O/acetone, 60 °C, 4h, 91 %. d) Di-(2-ethylhexyl)amine, DMF, $NaHCO_3$, Ar, 140 °C, 24 h, 58 %.

molecular structure of the assemblies while using the same solvent, $CDCl_3$. Some work has also been devoted to the hydrogen bond breaking effect of DMSO or methanol on hydrogen-bonded complexes in $CDCl_3$.[13] However, little attention has been paid to solvent effects on the same system. Owing to the remarkably high solubilities of monotopic perylene **5** and melamine **9** in all organic solvents, we were able to determine the influence of the solvent on the binding constant for complex **5·9** over a wide range of different solvent polarities. Apart from its high solubility additional advantages facilitated our studies: First, a well-defined 1:1 complex is formed when increasing amounts of melamine **9** are added to a solution of imide **5**. Second, the complexation process of perylene imide **5** can be monitored by different spectroscopic techniques including NMR-, UV/Vis- and fluorescence measurements, thus allowing widespread variations in the respective concentrations.

Upon complexation of perylene imide **5** by melamine **9**, the imide proton signal undergoes a significant downfield shift of several ppm in the NMR titration experiment, which is characteristic for hydrogen-bond formation (Figure 1).[4, 14–16] In contrast, in UV/Vis titration experiments comparatively small spectral changes are observed for the perylene chromophore (Figure 2). As we will show later, these spectral changes are mainly caused by hydrogen bonds from the

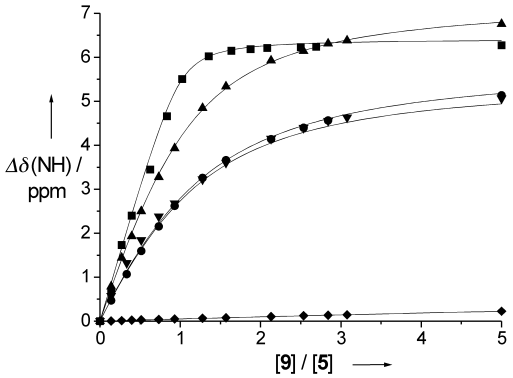

Figure 1. ^{1}H-NMR constant host titration data and calculated lines for the monotopic host **5** ($c = 7.0 \times 10^{-3}$ mol L^{-1}) and guest **9** in different solvents. ◆ [D_8]dioxane, ● $CDCl_3$, ▼ CD_2Cl_2, ▲ C_6D_6, ■ CCl_4.

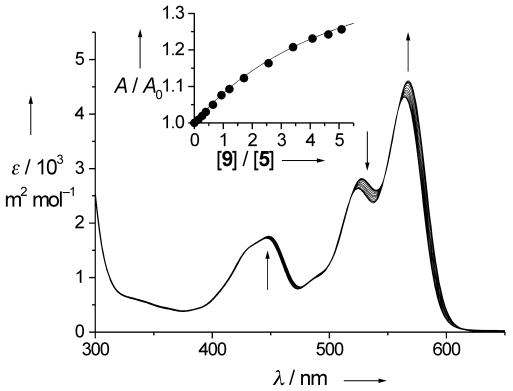

Figure 2. Changes in UV/Vis absorbance of monotopic perylene bisimide **5** (host) upon addition of melamine **9** (guest) in methylcyclohexane (host concentration: $c = 2.5 \times 10^{-5}$ mol L^{-1}). The arrows indicate increasing melamine concentration. Inset: Regression analysis at $\lambda = 590$ nm.

melamine NH protons to the imide oxygen atoms.[17] Even with these small changes accurate data evaluation was possible at several wavelengths, because melamine **9** does not exhibit interfering absorption bands beyond 300 nm. Similarly, fluorescence titration studies could be applied if the excitation and the detection wavelength were varied until a combination with a good signal-to-noise ratio was found. However, because of the low concentrations demanded in fluorescence spectroscopy this method is only useful for complexes of high binding strength.

As each method has its optimal concentration, the combination of these three techniques is appropriate to determine binding constants over a wide range, from about $K = 5-5000$ L mol^{-1} by NMR (corresponding to host concentrations of $0.1-10^{-4}$ mol L^{-1}), from $K = 1000-50\,000$ L mol^{-1} by UV/Vis ($10^{-3}-10^{-5}$ mol L^{-1}), and for $K > 10\,000$ L mol^{-1} by fluorescence spectroscopy ($< 10^{-5}$ mol L^{-1}). At the limiting concentrations both methods should be applied as different parts of the binding isotherm are covered by the respective experiments and the different spectral responses may be related to each other. The latter argument is of high importance to make sure that the same intermolecular contact, that is triple hydrogen bonding, takes place in all solvents studied.

As shown in Figure 1 and Table 1, the binding constant K and the resulting Gibbs binding energy ΔG^0 for the imide–melamine association reveal a dramatic dependence on the solvent. On changing from the moderately polar "standard" solvent chloroform to less polar solvents such as benzene, tetrachloromethane, and hexane, K increases by several orders of magnitude. At a first glance, this result might be rationalized by the mainly electrostatic nature of the hydrogen bond. Accordingly, the lowest binding constants are observed for the most polar solvent, tetrahydrofurane, and the highest value for the least polar solvent, *n*-hexane. For our approach to build up superstructures from perylene bisimides and melamines, the significant increase of K in the least polar aliphatic solvents will become of fundamental importance, because it allows stronger hydrogen bonding by simply changing the solvent which is by far easier than extending the binding motif to more elaborate systems such as quadruple hydrogen bonding.[18]

However, a closer look at the solvent dependence of K reveals that apart from solvent polarity (expressed in terms of the permittivity ε_r in Table 1), specific solvent-substrate interactions are important. This is impressively demonstrated by comparing the K values measured in dioxane, benzene, tetrachloromethane, and methylcyclohexane (MCH) which span the whole range from 20 up to 54 000 L mol^{-1} in spite of almost identical permittivities. Indeed, for dioxane one observes a similarly small binding constant as for the much more dipolar solvent THF. Obviously, not the permittivity of these solvents or the related dipole moments of the solvent molecules are the relevant quantities but the ability of ethers to act as hydrogen-bond acceptors, which compete for hydrogen bond formation with the complementary binding partners. This conclusion is also supported by the small change of the chemical shift δ_{NH}(imide) in ether solvents during the NMR-titration experiments compared with the other solvents (Figure 1). Also, for dichloromethane one might have expected a smaller value for K and ΔG than for chloroform due to the larger dipole moment. However, similar values are measured, which might be explained by the higher CH acidity of chloroform which provides weak hydrogen-bonding interactions to the basic oxygens of **5** and amino groups of **9**. Finally, in benzene a much smaller binding constant is

Table 1. Solvent dependence of binding constants K and Gibbs binding energies ΔG^0_{298} as determined by ^{1}H-NMR, UV/Vis and fluorescence titration experiments of the monotopic compounds **5** and **9**.

Solvent	ε_r	K [L mol^{-1}]	$-\Delta G^0_{298}$ [kJ mol^{-1}]	δ_{min}[a]	δ_{max}[a]	Method
[D_8]THF	7.58	15	6.5	10.87	12.48	NMR
[D_8]dioxane	2.21	20	7.4	10.56	11.97	NMR
$CDCl_3$	4.81	240	13.6	8.38	14.29	NMR
CD_2Cl_2	8.93	270	14.0	8.55	14.12	NMR
C_6D_6	2.27	1530	18.2	7.59	14.93	NMR
CCl_4	2.23	5080	21.1	8.20	14.61	NMR
CCl_4	2.23	4080[b]	20.6[b]			UV/Vis
MCH[c]	2.24	54 000[b]	27.0[b]			UV/Vis
MCH[c]	2.24	21 000[b]	24.7[b]			Fluores.
n-hexane	1.89	90 000[b]	28.3[b]			Fluores.

[a] As obtained from nonlinear regression analysis for the free (δ_{min}) and the bound imide protons (δ_{max}). [b] Average of data obtained for three different wavelengths ($\sigma = 0.6$ kJ mol^{-1}). [c] Methylcyclohexane.

0947-6539/00/0621-3874 $ 17.50+.50/0 *Chem. Eur. J.* **2000**, *6*, No. 21

determined than in tetrachloromethane, although both molecules have no dipole moment. However, benzene has a rather large quadrupole moment with a positive partial charge in the σ plane and a negative partial charge in the π planes. Again, this π basicity of the aromatic system might provide weak hydrogen bonding to the melamine and imide NH functionalities. Whereas all our observations are easily explained with chemical intuition the magnitude of the effect is hard to predict. It seems therefore of primary importance for supramolecular chemistry to have a closer look on solvent effects and to establish relationships for the most frequently used intermolecular interactions.

Further experiments were carried out with ditopic perylene bisimide **3b** and ditopic melamine **8b** to make sure that each of their receptor groups is able to bind the complementary binding partner. Figure 3 shows the results of the method of continuous variation of the perylene/melamine concentration in an NMR experiment for **3b·8b** and **5·8b** (Job's method).[14a] In both cases the highest amount of complexed imide is observed close to the theoretical value of 0.5 for **3b·8b** and 0.67 for **5·8b**. Similarly, the maximum of the Job plot for **3b·9** appeared close to 0.33. These results support the expected 2:1, 1:1 (= 2:2, respectively) and 1:2 stoichiometry for the given complexes.

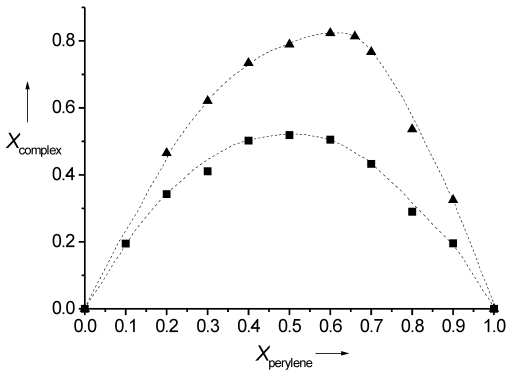

Figure 3. ^{1}H-NMR Job plots for ■ **3b·8b** and ▲ **5·8b** in chloroform: mole fraction of perylene bisimide **3b** or **5** bound to melamine **8b** ($X_{complex}$) as a function of the total mole fraction of perylene **3b** or **5** ($X_{perylene}$). The dotted lines are auxiliary.

In the next step, NMR titrations were carried out in $CDCl_3$ on these systems using the perylene derivative as the host and measuring the imide proton shift upon addition of increasing amounts of one of the melamines. All these experiments gave evidence for an essentially independent involvement of both receptor units of the ditopic receptors **3b** and **8b**, respectively, showing microscopic site binding constants of $K_\mu = 230\ L\,mol^{-1}$ ($\Delta G^0 = -13.5\ kJ\,mol^{-1}$) between **9** and **3b**, $K_\mu = 70\ L\,mol^{-1}$ between **5** and **8b** and $K_\mu = 60\ L\,mol^{-1}$ between **3b** and **8b** receptor groups.[19] Accordingly, identical binding strengths are given for ditopic perylene bisimide **3b** and monotopic perylene bisimide **5**, whereas melamine monoreceptor **9** exhibits a four times higher binding constant than ditopic melamine **8b**. As this change of K by a factor of four is exactly the value expected from statistical arguments (Scheme 5),[14, 15, 19] we may assume that no conformational preferences are present in **8b** and no energetically unfavorable rotations of the secondary amino groups around the N–$C_{triazine}$ bond precede the binding event.[20]

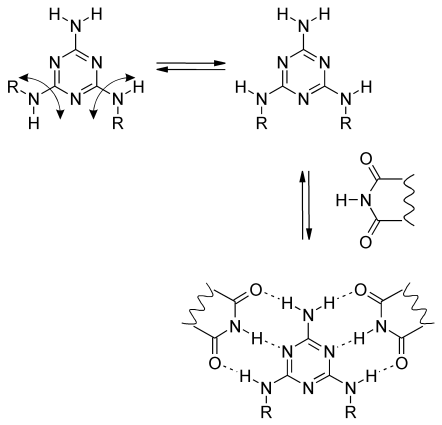

Scheme 5. Conformational equilibria in melamines **8a–c**. Because each RHN group may adopt two different orientations, only one of four possible structures is suited for complexation of two imides, which explains the reduced binding constant of **8a–c** compared with **9** by a statistical factor of four.

Due to the significantly lower solubilities of the ditopic perylene receptors **3a–c** compared with the monotopic receptor **5**, titration experiments involving **3a–c** could not be carried out in the less polar solvents. Nevertheless, based on identical binding strength of the imide units of perylenes **5** and **3a–c** and the decrease by a factor of four when changing from melamine monoreceptor **9** to ditopic receptors **8a–c**, binding constants between **3a–c** and **8a–c** may be calculated assuming a linear free energy relationship to the binding event measured for 1:1 complex **5·9** (Table 2, first column).

Supramolecular $[\cdot\cdot AA\cdots BB\cdot\cdot]_n$-type polymers: In an equimolar solution of a ditopic imide **3** and a ditopic melamine **8**, no complexes of defined composition and size are expected, but polydisperse assemblies $(\mathbf{3\cdot 8})_n$. For the given example, each building block possesses two identical binding sites complementary to those of the other unit. If the labels A and B are used for the two complementary receptor functionalities and A···B describes a single binding event characterized by a microscopic site binding constant K_μ, ditopic building blocks AA and BB are considered to associate to give a supramolecular polymer $[\cdot\cdot AA\cdots BB\cdot\cdot]_n$. This situation compares to some extent to nylon-type condensation polymerization where a polymer is formed by the reaction between two bifunctional building blocks. However, in contrast to polycondensation reactions, no covalent bond is formed in the supramolecular polymer and the chain formation process is fully reversible and highly dependent on the magnitude of the binding constant and the concentration. If we assume independent binding events for each interaction between the complementary receptors A and B (that means equal binding constants K_μ for each association between A and B), the mean degree of polymerization ($\overline{DP}$) for such a supramolecular polymer can be calculated for a given binding constant and concentration. The result of such a treatment has already been described for the simpler situation of an $[\cdot\cdot AA\cdot\cdot]_n$ type supramolecular polymer with only one type of

self-complementary receptors characterized by a binding event A ··· A.[13a, 18] For the case of a $[\cdot\cdot AA\cdots BB\cdot\cdot]_n$ polymer one has additionally to take into account stoichiometry, that is any deviation from an exact 1:1 ratio of the two building blocks will cause a substantially diminished mean chain length.[21] In order to describe this situation, we could derive Equation (1) (see Supporting Information), where $\overline{DP}$ is the mean chain length or degree of polymerization of the supramolecular polymer, c_A^0 and c_B^0 are the total concentrations of the receptor units (i.e., $c_A^0 = 2c_{AA}^0$ and $c_B^0 = 2c_{BB}^0$), and K_μ is the microscopic site binding constant. With stringent stoichiometry ($c_A^0 = c_B^0$), Equation (1) simplifies into Equation (2), which is the supramolecular version of the well-known Carothers' Equation of condensation polymer chemistry. Here, p denotes the probability for a receptor A or B to be bound. It is noteworthy that this Equation is also applicable to $[\cdot\cdot AB\cdot\cdot]_n$ (perlon-type) supramolecular polymers which were recently introduced by Gibson et al.[22]

$$\overline{DP} = \frac{\text{number of monomers}}{\text{number of assemblies}} = \frac{(c_A^0 c_B^0)^2}{2c_A^0\left(-\frac{1}{K_\mu} + \sqrt{\left(c_A^0 + c_B^0 + \frac{1}{K_\mu}\right)^2 - 4c_A^0 c_B^0}\right) + (c_B^0)^2 - (c_A^0)^2} \quad (1)$$

$$\overline{DP} = \frac{1}{1-p} = \frac{2c_A^0}{-\frac{1}{K_\mu} + \sqrt{\left(2c_A^0 + \frac{1}{K_\mu}\right)^2 - 4(c_A^0)^2}} \quad (2)$$

Equation (1) provides a general formula for single-chain supramolecular polymers formed through reversible association of AA- and BB-type ditopic receptors. Long-chain assemblies are only predicted for an exact stoichiometry of the two receptors A and B, whereas for unequal stoichiometry the chain length drops rapidly to one (for a plot see Supporting Information). Even for an exact stoichiometry long chains of associated molecules are only obtained at high concentrations and for high binding constants. Thus, the binding constant has to be at least 50000 $L\,mol^{-1}$ to afford polymer-like properties at practical concentrations. From Equation (1) we conclude that each order of magnitude enhancement of the K value will allow polymeric properties to be observed at about one order of magnitude lower concentration. If we consider the challenge of designing systems which exhibit such high association constants it is not surprising that only a small number of supramolecular polymers have been described until now[18, 22, 23] (note that three-dimensional complexation as in host–guest chemistry is not feasible in the given situation). From the experimental point of view, these findings also imply very high demands on the purity of the compounds and the exact stoichiometry of the two components. This explains why our synthesis required an additional purification step involving chromatography of Boc-protected bisimides.

These theoretical considerations could now be applied to our bisimide–melamine system **3·8** using the binding constants calculated for the various solvents. As shown in Table 2, concentrations of at least 10^{-2} $mol\,L^{-1}$ (which corresponds to 15 $g\,L^{-1}$ for **3b·8b**) of an exactly stoichiometric mixture of the ditopic receptors **3** and **8** are required to achieve a considerable percentage of bound receptors for the majority of solvents studied. Eventually, only for aliphatic solvents, for example methylcyclohexane, the transition from oligomeric to polymeric chains takes place giving a considerable degree of polymerization.

Table 2. Degree of polymerization ($\overline{DP}$) for perylene–melamine complexes $(\mathbf{3\cdot8})_n$ in dependence of the receptor concentration and the solvent according to Equation (1) or (2).

Solvent	K_μ [$L\,mol^{-1}$][a]	c [$mol\,L^{-1}$][b]	% Complexation	$\overline{DP}$[c]
THF	4	2×10^{-2}	7	1.1
dioxane	5	2×10^{-2}	8	1.1
$CHCl_3$	60	2×10^{-2}	41	1.7
CH_2Cl_2	70	2×10^{-2}	44	1.8
C_6H_6	380	2×10^{-2}	70	3.3
CCl_4	1270	2×10^{-2}	82	5.6
MCH[d]	13500	2×10^{-2}	94	16.9
MCH[d]	13500	2×10^{-3}	83	5.7
MCH[d]	13500	2×10^{-4}	55	2.2
MCH[d]	13500	2×10^{-5}	18	1.2

[a] Assuming a linear free energy relationship for triple hydrogen-bond formation between (**5·9**) and (**3·8**). [b] $c = c_A^0 = c_B^0 = 2\times[\mathbf{3}] = 2\times[\mathbf{8}]$. [c] $\overline{DP} = 2n$. [d] Methylcyclohexane.

Finally, it is important to note that this treatment describes the growth of the polymeric chain only based on one single binding event of high specificity, that is triple hydrogen bonding between the individual molecules. For chloroform and other chloroaliphatic solvents, our considerable number of binding studies using NMR- and optical techniques provide reasonable evidence for such a situation because here hydrogen bonding is the only effective interaction over the whole concentration range from 10^{-6} to 10^{-2} $mol\,L^{-1}$. Other types of intermolecular interactions between the given building blocks are lower by orders of magnitude. However, additional intermolecular interactions become important in other solvents or in the solid state as will be discussed in the next part of the paper.

π–π Aggregation and hierarchical growth in solution: The absorption spectra of perylene bisimide dyes **3**, **5**, and **6** show two distinct bands in the UV/Vis range (Figure 2). According to Reisfeld[24] these absorption bands are assigned to two different electronic transitions, the S_0-S_1 from 480 to 600 nm and the S_0-S_2 from 400 to 460 nm. The S_0-S_1 transition is of high intensity with a transition dipole moment of 2.0×10^{-29} C m (oscillator strength $f = 0.3$) and a polarization directed along the long molecular axis. The vibronic states exhibit an energy order of $\approx$1300 cm^{-1} which is typical for the perylene skeletal vibrations. In contrast, the higher energy electronic S_0-S_2 transition is not observed for perylene bisimides without substituents in the bay region.[8] Its transition moment is polarized perpendicularly to the S_0-S_1 transition and its intensity depends on the respective substituents at the central part of the chromophore. According to ZINDO/S MO calculations, both the HOMO and the LUMO orbital of perylene–bisimide dyes exhibit nodes at the imide nitrogens which explains that the substituents at this atom do not influence the optical properties of the chromophore.[17] On the other hand, the imide oxygens exhibit a significant amplitude for both frontier orbitals. The bathochromic shift

  0947-6539/00/0621-3876 $ 17.50+.50/0 *Chem. Eur. J.* **2000**, *6*, No. 21

and the increase of the lowest energy vibronic band upon complexation of the imides with melamines are thus attributed to the polarization of these imide oxygen atoms by hydrogen bonding (Figure 2).

Whereas the same minor changes in the absorption spectra are observed in dilution studies of the **5·9** 1:1 and the **9·3b·9** 1:2 systems in all solvents, significant differences are revealed in a dilution experiment of the ditopic couple **3b·8c** in the least polar aliphatic solvents, for example methylcyclohexane (Figure 4). As for **5·9**, the lowest energy transition is shifted bathochromically (≈3 nm) due to hydrogen-bond formation to the melamines. In addition, however, strong changes in the intensities of the vibronic transitions of the S_0-S_1 as well as the intensity of the S_0-S_2 absorption band are observed. Thus, for the S_0-S_1 band an additional shoulder appears at 600 nm and the higher energy vibrational transitions gain energy at the expense of the formerly strongest transition at 560 nm. For the perpendicular S_0-S_2 transition we note a significant decrease in intensity. Clearly, these changes cannot be explained by hydrogen bonding to the peripheral imide moieties alone, but suggest additional contributions resulting from $\pi-\pi$ interactions (excitonic coupling) and/or alterations in the intensity of the vibronic transitions due to geometrical changes, for example aggregation-induced planarization of the chromophores. It is known for flat perylene derivatives having no substituents in the central part of the molecule that aggregation of the π systems will occur at higher concentrations giving rise to pronounced excitonic coupling of the optical transitions.[25, 26] However, the significant twisting of perylene bisimides **3b** due to the four phenoxy substituents as well as the bulky *tert*-butyl groups will counteract such π stacking of the perylenes' aromatic surfaces.[27] This is clearly demonstrated by bisimide **6** which does not show any change in the absorption spectrum over the concentration range from 10^{-4} to 10^{-6} mol L^{-1} in methylcyclohexane. Also in dynamic light scattering (DLS) measurements no aggregation could be observed for **6**.

Identical concentration dependent changes in the absorption spectra as for **3b·8c** are also observed with melamine **8b** while the shorter chain melamine **8a** could not provide the required solubility to the complex to enter the relevant concentration range. On the other hand, for **3c·8b** and **3c·8c** bearing the bulkier *tert*-octylphenoxy-substituents a concentration of 5×10^{-5} mol L^{-1} could be achieved but only the bathochromic shifts as depicted for the monotopic model system **5·9** (Figure 2) were observed which points to hydrogen bonding as the only significant interaction. It is also remarkable that the solubilities of *tert*-butylphenoxy assemblies **3b·8b, c** in methylcyclohexane were higher by more than one order of magnitude than those of *tert*-octylphenoxy assemblies **3c·8b, c**, despite of the usually more solubilizing *tert*-octyl substituents. Because of their much lower solubilities, complexes containing perylene bisimide **3a** could not be studied in methylcyclohexane solution in the required range of concentration.

From the given observations, it seems clear, that the changes in the absorption spectra shown in Figure 4 reveal a unique process taking place only for assemblies of *tert*-butylphenoxy-substituted bisimides **3b** with long-chain melamines **8b, c** in an aliphatic surrounding at a concentration between 10^{-5} and 10^{-3} mol L^{-1}. As shown in Table 2, this range corresponds exactly to the concentration where hydrogen bonding starts to take effect and an association process to oligomeric species evolves. These oligomers bear extended aromatic surfaces constrained in a rather rigid geometry due to the triple hydrogen bonding between the building blocks. For such a situation, numerous small $\pi-\pi$ interactions may sum up to significant forces which drive the assembly in a second dimension leading to three-dimensional growth to a mesoscopic system. Although these secondary $\pi-\pi$ interactions are weaker than the melamine-imide hydrogen bonds, both association processes occur simultaneously above a critical concentration as revealed by a number of well-defined isosbestic points at 467, 541, and 581 nm (Figure 4). This observation indicates a cooperative process in which the evolving hydrogen-bonded polymeric chains aggregate to an extended three-dimensional supramolecular system of enhanced stability compared with a purely one-dimensional hydrogen-bonded chain (Scheme 1).

To support this point of view additional calculations and experiments were carried out. First, we applied our model of independent receptor sites (see above) to gain the best possible fit to the experimentally observed concentration dependence of the absorption data for **3b·8c**. As shown in the inset of Figure 4, the experimental data exhibit a more pronounced change in absorption around the critical concentration 3×10^{-5} mol L^{-1} than the calculated line, which is a clear sign of cooperativity. Moreover, in contradiction to the simple association equilibrium described by Equation (2), the self-organization process of **3b·8c** is fully completed already at a concentration of about 3×10^{-4} mol L^{-1}, which is at least one order of magnitude lower than we expected for a simple hydrogen-bonded system with $K_\mu = 13\,500$ L mol^{-1}. At least this argument holds true for those interactions which affect the optical transitions of the perylene chromophore which do not change anymore at higher concentration.

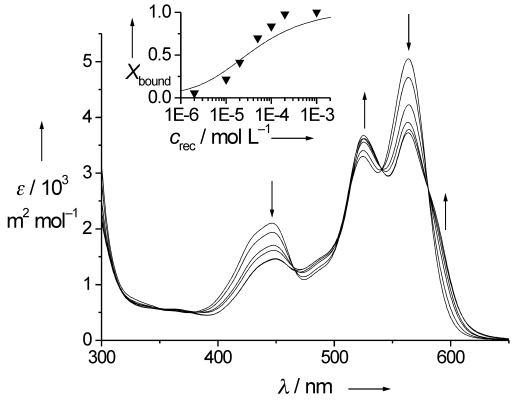

Figure 4. Concentration dependent UV/Vis absorption spectra in methylcyclohexane for a stoichiometric mixture of perylene bisimide **3b** and melamine **8c** ($c = 10^{-6}$ to 10^{-4} mol L^{-1}). Arrows indicate changes upon increasing concentration. Inset: Fraction of bound receptors according to the experimental values at 525 nm (▼) and a line-fitting analysis based on a simple 1:1 model (solid line).

Second, temperature-dependent UV/Vis absorption studies of a 5×10^{-5} mol L^{-1} solution of **3b·8c** afforded the same spectral changes as observed in the dilution experiment (Figure 5). This is reasonable because the association constant decreases upon heating due to the higher contribution of entropy to ΔG. When the temperature was increased beyond 40 °C the perylene bisimide precipitated in form of a violet film on the cell. This behavior is explained by the low solubility of free **3b** in methylcyclohexane which will not persist in solution without being bound to melamines by hydrogen bonds. Similar processes are observed in biological systems, as for example DNA melting or protein denaturation. If the extinction coefficient at a given wavelength is plotted against temperature, a sigmoidal graph is obtained, again indicating a cooperative process (Figure 5, inset). Because of the complicated equilibria and an even larger number of parameters involved than for the dilution experiment, we were not able to evaluate this experiment quantitatively. However, from the point of inflection a melting temperature of $\approx$35 °C is deduced for assemblies $(\mathbf{3b \cdot 8c})_n$ and a fairly good fit of the data is noted if a formula used for DNA melting studies is applied to our data.[28, 29]

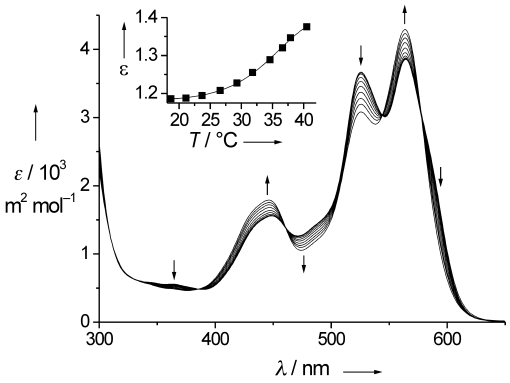

Figure 5. Temperature dependence of UV/Vis absorption spectra of a 5×10^{-5} mol L^{-1} solution of perylene bisimide **3b** and melamine **8c**. Temperature range 18.7–40.5 °C, arrows indicating increasing temperature. At higher temperatures, **3b** precipitated. Inset: Change of absorption at 445 nm (■) and calculated line according to a common model used for DNA melting studies.[28]

Finally, the molecular assemblies have been characterized in dilute solution by dynamic light scattering (DLS).[30] Here, for a 5×10^{-5} mol L^{-1} stoichiometric solution of perylene bisimide **3b** and melamine **8c** in methylcyclohexane distinct correlated scattering could be observed with an angle dependence of the characteristic relaxation time that points to particles of nonspherical shape. The time intensity correlation functions could be analyzed with a stretched exponential decay, with stretching parameters $\beta = 0.75 - 0.80$, corresponding to a size polydispersity of the particles larger than 50 %. In addition, the inverse apparent hydrodynamic radius $R_{app}(q)^{-1}$ showed a nonlinear decrease by more than a factor of two with decreasing scattering vector q in all cases, as shown in Figure 6.

By interpolation of the data to $q = 0$, as indicated by the bold arrow in Figure 6, the z-average hydrodynamic radius of the aggregates was determined to be about 200 nm. This value

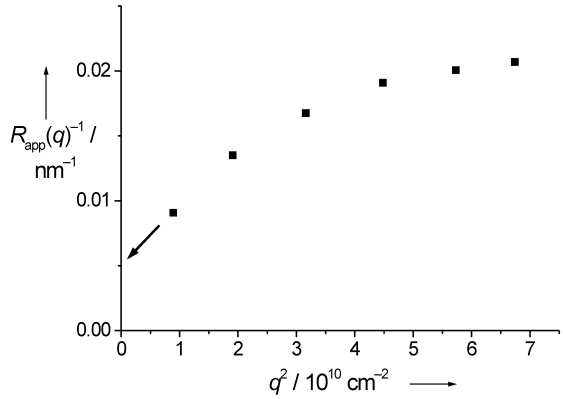

Figure 6. Inverse apparent hydrodynamic radius $R_{app}(q)^{-1}$, determined from fitting the time intensity correlation functions $G_2(q,t)$ according to Equation (4) (see Experimental Section) versus the square of the scattering vector q.

is about two orders of magnitude larger than the average size of the single dye and melamine components, and therefore demonstrates the formation of extended superstructures already in dilute solution. For comparison, the dimension of the repeating unit of **(3b·8c)** given in Scheme 1 is about 2.0 nm × 3.5 nm assuming extended C_{18} alkyl chains.

In a second experiment, the effect of increasing amounts of monotopic melamine **9** on the size of $(\mathbf{3b \cdot 8c})_n$ assemblies has been studied by DLS and the resulting apparent hydrodynamic radii determined at scattering angle $\theta = 50°$, have been summarized in Table 3. Notably, the size of the aggregates does not change with the first small fraction of added **9**, but then immediately drops below the experimental resolution of the DLS technique which means that the particles in solution are now smaller than 1–2 nm in hydrodynamic radius. Here, it should be mentioned that also no scattering particles could be observed for pure 5×10^{-5} mol L^{-1} solutions of perylene bisimide **6** in methylcyclohexane, emphasizing the important role of ditopic melamines for the formation of extended supramolecular assemblies.[31]

Table 3. Apparent hydrodynamic radius R (at a scattering angle $2\theta = 50°$) for samples containing 5×10^{-5} mol L^{-1} of **3b·8c** in methylcyclohexane and increasing amounts of melamine **9** as a chain-terminating agent.

Concentration of **9** [mol L^{-1}]	Receptor ratio for **9**/**8c**	R ($2\theta = 50°$) [nm]
0	0	100
1×10^{-5}	0.1	100
3×10^{-5}	0.3	< 2
1×10^{-4}	1	< 2
2.5×10^{-4}	2.5	< 2

To explain the dependence of the particle size on the amount of added melamine **9** we have to consider exchange equilibria between the two melamines **8c** and **9**, respectively, and bisimide **3b**. The original solution contains 5×10^{-5} mol L^{-1} **3b** and **8c** which form extended assemblies of high structural anisotropy with an averaged hydrodynamic radius of about 200 nm. Therefore, the degree of complexation for **3b** and **8c** is almost quantitative and most **3b** and **8c** molecules are assembled in these particles. However, upon

0947-6539/00/0621-3878 $ 17.50+.50/0 *Chem. Eur. J.* **2000**, *6*, No. 21

addition of the monotopic compound **9**, the two melamines **8c** and **9** compete for the imide binding sites of the perylene dyes. Our binding data suggest that **9** has a somewhat higher binding affinity for imides than **8c** in chloroform, but this situation might be different in aliphatic solvents in the presence of additional $\pi-\pi$ interactions. Nevertheless, already a small percentage of exchanged melamines will lead to significantly smaller hydrogen-bonded chains owing to the chain terminating properties of the monotopic receptor **9**. Obviously the critical concentration is given at about 2×10^{-5} mol L^{-1} melamine **9**, where the hydrogen-bonded chain is shortened to such an extent that the capabilities for three-dimensional growth involving extended π surfaces are lost. This interrelationship between particle size and $\pi-\pi$ aggregation is also confirmed by spectral changes similar to those given in Figure 4 when **9** was titrated into a solution of **3b·8c** in an UV/Vis experiment (see Supporting Information). From these studies we may conclude that **9** has a similar effect on $(\mathbf{3b\cdot8c})_n$ assemblies as urea has on the secondary and tertiary structure of proteins, that is it induces denaturation.

Mesoscopic strands of 3b·8b, c in the solid state: When a 5×10^{-5} mol L^{-1} methylcyclohexane solution of equimolar composition in perylene **3b** and melamine **8b** or **8c** is evaporated on a formvar/carbon coated grid, a dense network of intertwined cylindrical strands is formed (Figure 7). Visualization by transmission electron microscopy (TEM) can be achieved by staining either with uranyl acetate or with osmium tetroxide. As uranyl acetate is applied in an aqueous solution, but osmium tetroxide is deposited in the gas phase, we conclude that the formation of the mesoscopic superstructures is not affected by the staining process, because both procedures lead to the same result.[32] After sputtering the TEM grid with a 5 nm chromium layer, the strands can also be investigated by scanning electron microscopy (SEM).

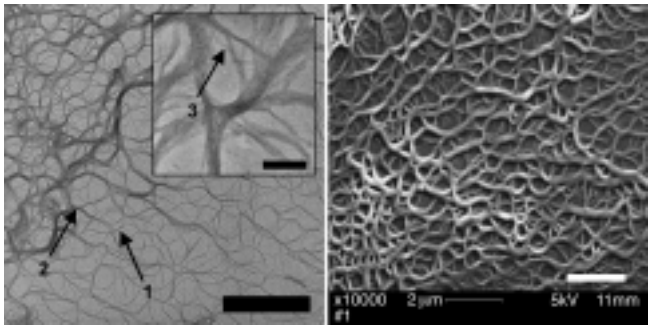

Figure 7. Left: Transmission electron micrographs of mesoscopic superstructures of **3b·8b** after evaporation of a methylcyclohexane solution on carbon/formvar-coated nickel grids (200 mesh) and staining with uranyl acetate. The length of the scale bar is 2000 nm. The inset shows a magnification (scale bar 250 nm). Right: Scanning electron micrograph of **3b·8b** after sputtering with a 5 nm chromium layer. The length of the scale bar is 2000 nm.

As seen in Figure 7, strands from about 20 nm up to 500 nm in diameter which extend over several micrometers are formed. Whereas our light-scattering experiments already gave evidence for the existence of large-sized aggregates in 5×10^{-5} mol L^{-1} solution further assembly took place with increasing concentration during the evaporation process leading to a highly intertwined network of merging individual strands. The majority of the strands exhibit diameters of ≈100 nm (arrow 1) which may combine to thicker units having diameters of 250 nm (arrow 2) or even larger. At a higher magnification (inset of Figure 7 left) numerous smaller structures are revealed with a diameter of ≈15 nm (arrow 3). We note that this is still an order of magnitude larger than the diameter of the constituent molecular building blocks of **3b** and **8b**. A better spatial impression of these structures is provided by SEM (Figure 7 right) which reveals a cylindrical cross-section of the strands. However, due to the sputtering technique with 5 nm chromium, the smaller structures are not visible in SEM anymore. In contrast to **3b·8b, c**, perylene–melamine aggregates **3c·8b** and **3c·8c** which do not exhibit $\pi-\pi$ aggregation did not show superstructures. Based on these results an unambiguous relationship between the microscopically observed superstructures in TEM and SEM and the aggregation process on the molecular level detected by UV/Vis dilution experiments is established. Only those assemblies **3b·8b, c** which exhibit the second interaction involving the π systems of the hydrogen-bonded chains afford extended mesoscopic superstructures visualized by electron microscopy.

The same superstructures also formed on glass slides which were previously made hydrophobic by treatment with trimethylchlorosilane. On untreated glass surfaces, only irregular precipitates are observed, probably due to the interaction of the polar imide and melamine functionalities with the OH groups of the surface which compete for the hydrogen bonds. Visualization of these structures was achieved by laser scanning confocal microscopy (LSCM) as will be discussed later in the context of the optical properties of the assemblies. Thicker homogeneous films of **3b·8b** or **3b·8c** which were prepared in a similar manner on silanized glass slides reveal textures under an optical polarization microscope at crossed polarizers. As these textures do not match textures of common liquid crystals, we cannot attribute them to a certain type of supramolecular ordering yet.

It is tempting to speculate on the molecular order of the mesoscopic assemblies shown in Figure 7. Based on crystal structures of a number of combinations of ditopic barbituric acids and ditopic melamines Whitesides and co-workers[4a] could prove the existence of zigzag chain ("tape") and cyclic ("rosette") or helical motifs and establish some general trends which relate the preferred motif to the size of the substituents attached to the melamine and barbituric acid building blocks. For **3b·8b, c** the most likely structural motifs are zigzag chains which are, however, not planar because of the twisting of the perylene subunits.[27] Such chains might aggregate through $\pi-\pi$ interactions giving highly ordered microdomains as suggested by the isosbestic points of Figure 4 and preferred diameters and curvatures of the structures in Figure 7. On the other hand, the disorder introduced by the twisting of the perylene subunits will limit the dimension of ordered domains and create linear and curved topologies and branching of the mesoscopic strands.[33] Thus, despite of a number of arguments for structural order at the molecular

level, that is isosbestic points in Figures 4 and 5, macroscopically irregular networks are formed.

Fluorescence properties: As pointed out in the introduction, our main interest in perylene-based assemblies is driven by the prospect of new nanoscopic functional materials derived from building blocks which are organized in space by distinct supramolecular interactions. Energy migration phenomena in such assemblies might be an especially intriguing application which could be of significance in the context of artificial light harvesting. As a first step towards this goal we investigated the fluorescence properties of perylene bisimides **3b** and **5** in their uncomplexed, hydrogen-bonded and aggregated states. Both dyes exhibit fluorescence quantum yields higher than 0.90 in different solvents (Table 4). The fluorescence spectra are mirror images relative to the S_0-S_1 absorption band, with a Stokes shift of about 30–40 nm for the 0–0 transition. For

Table 4. Fluorescence quantum yields Φ_f and peak positions λ_e for perylene bisimide dyes **3b** and **5** in different solvents.

	MCH	Dioxane	Benzene	CH_2Cl_2	Isopropanol
3b Φ_f	0.93	0.95	0.93	0.98	0.86
λ_e [nm]	592	599	604	614	613
5 Φ_f	0.94	0.95	0.93	0.93	0.87
λ_e [nm]	593	600	604	614	615

polar solvents, the fluorescence peak position shifts to higher wavelengths, and a larger Stokes shift is observed. Interestingly, for dioxane, which is a strong hydrogen-bond acceptor (see NMR titration experiment), the same high fluorescence quantum yield is observed as for the non hydrogen-bonding solvents. On the other hand, for isopropanol which can act as a hydrogen-bond donor, slightly lower quantum yields are given. It is likely that these differences are again caused by the HOMO and LUMO orbitals which exhibit density at the hydrogen bond acceptor oxygens, but nodes at the hydrogen bond donating nitrogens.[17] Because of these nodes, hydrogen-bonding interactions of dioxane with the imide proton do not affect the fluorescence properties in contrast to isopropanol which interacts with the carbonyl oxygens.

Similar changes in absorption and emission properties are observed upon hydrogen bond complex formation between the monotopic perylene dye **5** and the monotopic melamine **9**, which was examined by titrating **5** with **9** in methylcyclohexane (Figure 8). With increasing amounts of melamine added, absorption and fluorescence bands shift to longer wavelengths. Based on selected pairs of excitation and detection wavelengths rather strong changes in fluorescence intensity are detected which are suited to deduce the binding constants (vide infra). In the given experiment, however, our interest was in the change of the fluorescence intensity which was obtained through integration of the fluorescence spectra and calibration against the respective fluorescence standard dye. As can be seen from Figure 8 (triangles, solid line), the hydrogen-bonded perylene bisimide still exhibits 90% of the fluorescence intensity of the free chromophore. Thus, the fluorescence quantum yield of the hydrogen-bonded complex **5·9** is still 0.80 showing that hydrogen bonding is no major

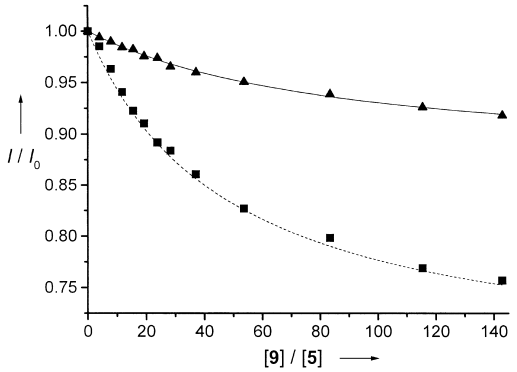

Figure 8. Change of the relative fluorescence intensity of perylene bisimide **5** ($c = 10^{-6}$ mol L^{-1}) in methylcyclohexane in the presence of increasing amounts of melamine **9** as obtained by integration (▲, solid line) and the intensity at a detection wavelength of 610 nm (■, dashed line) in a fluorescence titration experiment (excitation wavelength 530 nm). The full set of absorption and emission spectra is given in the Supporting Information.

radiationless deactivation path for excitation energy in hydrogen-bonded perylene bisimide–melamine assemblies. This is a remarkable result, because there are numerous examples where optical excitation is followed by rapid proton migration causing efficient fluorescence quenching ("Förster cycle").[34]

Next, we became interested in the effect of $\pi-\pi$ aggregation upon the fluorescence properties. This was considered to be an especially crucial point because $\pi-\pi$ interactions are known to be very favorable for electron migration, which is a highly competitive photophysical process to energy migration. Accordingly, methylcyclohexane solutions of **3b·8c** in the concentration range of $10^{-6}-10^{-4}$ mol L^{-1} were investigated by fluorescence spectroscopy. Owing to the high optical densities of the solutions required for substantial aggregation, no fluorescence quantum yields could be determined for the aggregates using the conventional optically dilute method and a right angle setup. Instead, the front-face illumination technique was applied on a 1 mm cell and calibration was accomplished using methylcyclohexane solutions of the non-aggregating perylene bisimide dye **6** ($\Phi_{f,MCH} = 0.96$) at the same concentrations and under the same experimental conditions (Figure 9d). For this compound, the emission fine structure and peak position remain unchanged, but for the higher concentrations, the observed fluorescence intensity shows a nonlinear dependence on the concentration. This deviation from linearity could be fully described by Equation (3), given in the Experimental Section.

In contrast to **6**, the dependence of fluorescence position, fine structure and intensity on concentration is more complex for **3b·8c** assemblies. As seen in Figure 9a–c, all fluorescence spectra of methylcyclohexane solutions of **3b·8c** show a close mirror image behavior to the S_0-S_1 absorption band similar to simple molecular perylene derivatives.[5, 8, 24] The more dilute solutions where only small aggregates are present, exhibit fluorescence intensities comparable to the corresponding solutions of **6**. However, upon increasing the concentration to 10^{-4} mol L^{-1}, the intensity drops to 19% of the value obtained for **6** (Figure 9d). At the same time the

0947-6539/00/0621-3880 $ 17.50+.50/0 *Chem. Eur. J.* **2000**, *6*, No. 21

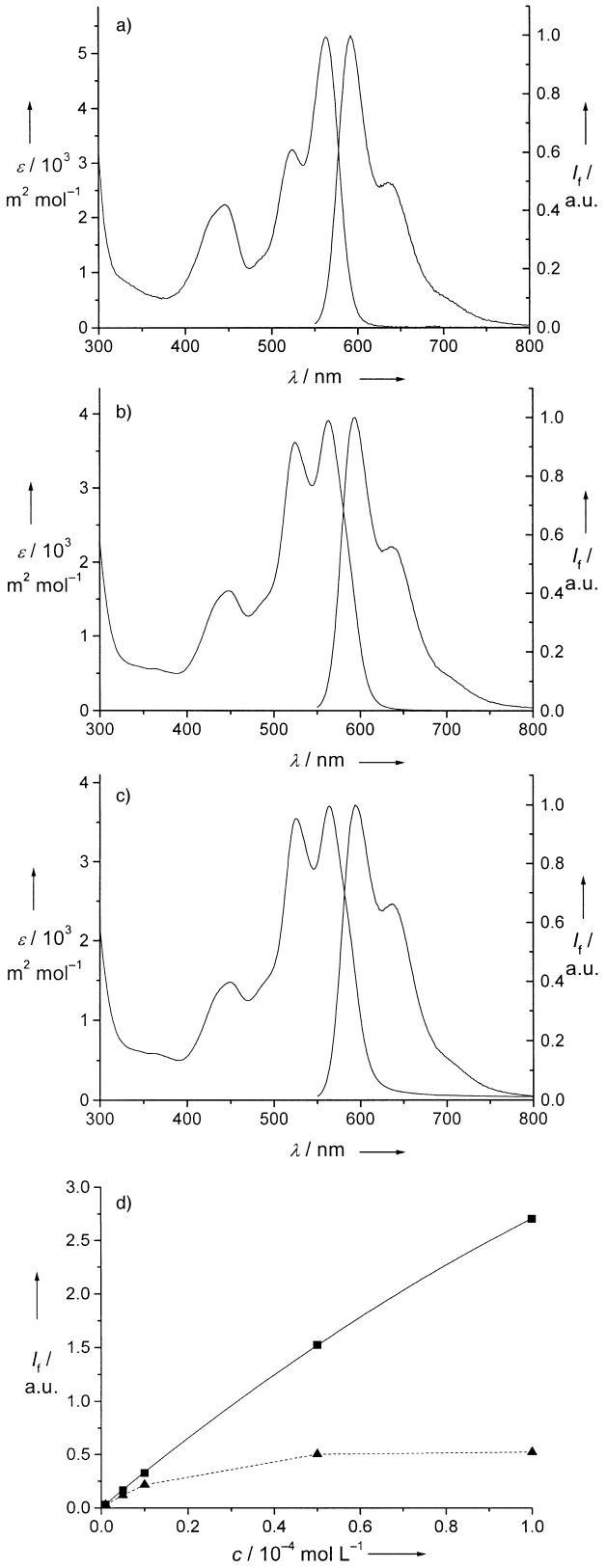

Figure 9. Concentration dependence of absorption and emission spectra of equimolar complexes of perylene bisimide **3b** and melamine **8c** in methylcyclohexane: a) 10^{-6} mol L^{-1}, b) 5×10^{-5} mol L^{-1}, c) 10^{-4} mol L^{-1}. d) Fluorescence intensity of methycyclohexane solutions of **6** (■) and **3b·8c** (▲). For **6**, the data points could be fitted according to Equation (3) (see Experimental Section). For **3b·8c**, the data points are connected by an auxiliary line. The excitation wavelength for fluorescence spectra was 530 nm.

long-wavelength shoulder at 637 nm gains considerably in intensity with respect to the emission maximum at 594 nm (Figure 9c). The observed loss in fluorescence intensity and the changes in the spectral fine structure could be related to light scattering (compare above) or π–π aggregation. For π–π aggregated chromophores incorporated into extended assemblies, fluorescence properties of solid particles (described below) are expected and not those of small assemblies in solution. In this context it is interesting to note the significant increase of the second long-wavelength emission band at 637 nm compared with the shorter wavelength maximum at 594 nm with increasing concentration. Because this long-wavelength emission band occurs at the same spectral position as observed for thin solid films (Figure 10), it is likely that this band is the major emission band of the aggregated dyes whereas the maximum at shorter wavelength comes from smaller hydrogen-bonded assemblies which exhibit higher fluorescence quantum yields and therefore contribute to a larger extent to the resulting fluorescence spectra in solution than the fluorophores incorporated into the large π-aggregated particles.

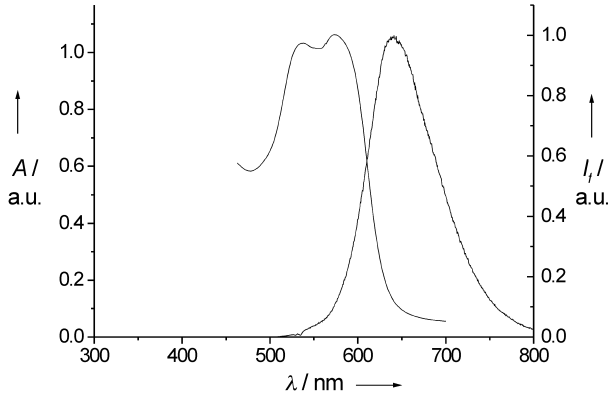

Figure 10. Absorption and emission spectra of a film of assemblies **3b·8c** on silanized glass.

Finally, solid state optical properties were studied for the mesoscopic strands by absorption and fluorescence spectroscopy and confocal fluorescence microscopy. These studies became possible because of the excellent photostability of these perylene–melamine superstructures which do not show any bleaching even after multiple scans of the same area of the sample in the confocal microscope. The sample preparation followed the procedure used for electron microscopic studies, that is 5×10^{-5} mol L^{-1} solutions of **3b·8c** in MCH were slowly evaporated on a hydrophobic surface which was now a silanized glass slide. As shown in Figure 11, a dense network of fluorescent strands is observed which is fairly related to the TEM and SEM micrographs. Owing to the lower resolution of the confocal microscope of ≈200 nm we cannot distinguish between smaller and larger strands but we note some variations in the fluorescence intensity. Figure 10 shows the absorption and emission spectra of such a sample. Both exhibit evidence of energetic disorder of the individual chromophores given by an inhomogeneous line broadening and an increased Stokes shift. The latter effect might be

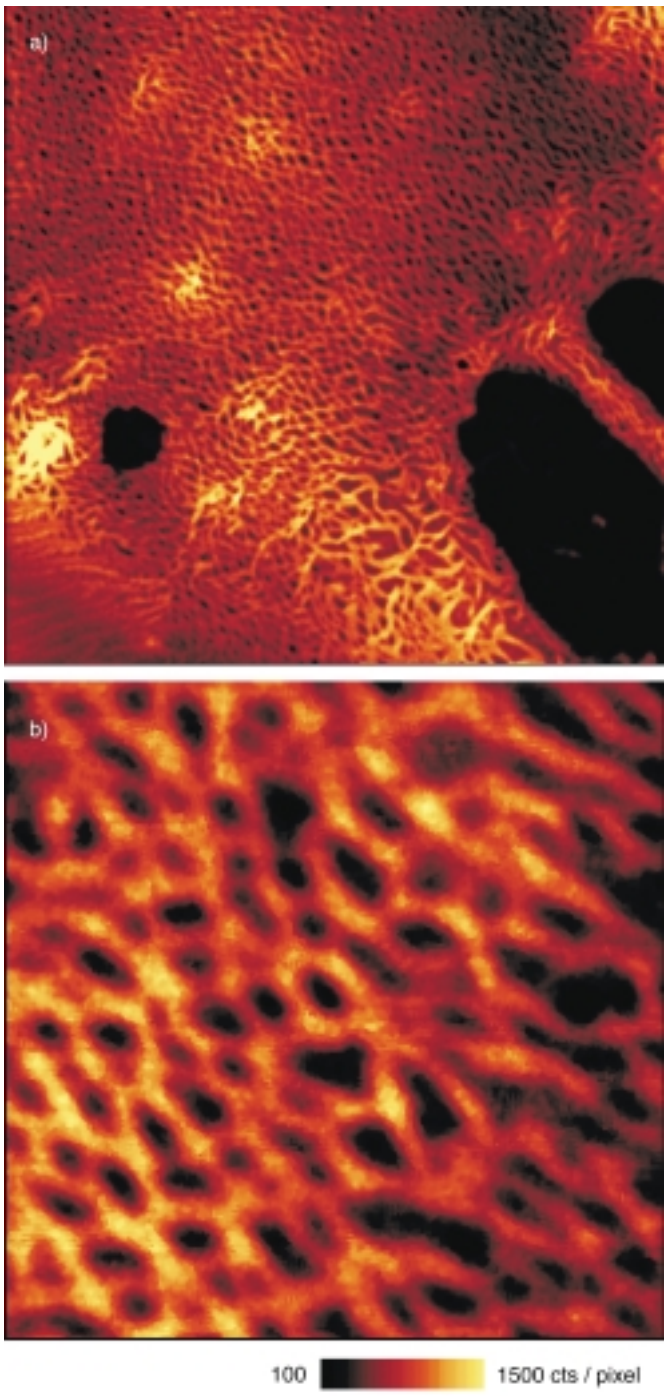

Figure 11. Confocal fluorescence micrographs of mesoscopic superstructures of **3b·8c** on silanized glass at different magnifications. Excitation 40 μW at 543 nm, filter RG 590, time per pixel 2 ms. Fluorescence intensity 100–1500 counts per pixel. Image size a) 50 μm × 50 μm, b) 10 μm × 10 μm.

explained by energy transfer processes between the exciton-coupled dyes which lead to spectral relaxation to the low-energy tail of the original dye emission spectrum.[35] Closer insight into the spectral properties of the mesoscopic strands was provided by spatially resolved fluorescence spectroscopy. For this purpose, 128 × 128 spectra were recorded from a 20 μm × 20 μm area of the sample.

As can be seen from Figure 12, lines a) and b), the emission maximum varies from 639 nm to 651 nm when moving from the areas with low fluorescence intensity between the strands to the center of the strands, where the highest intensity is detected. Also the line broadening is somewhat reduced and the Stokes shift is increased for the supramolecular strands

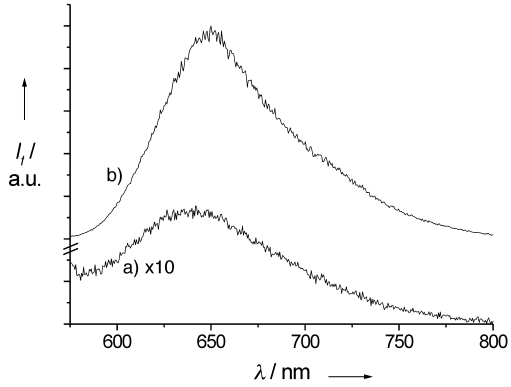

Figure 12. Spatially resolved fluorescence spectra of the mesoscopic superstructures of **3b·8c** on silanized glass. From a 20 μm × 20 μm area of the sample, 128 × 128 spectra were taken. For each graph, 20 representative spectra were averaged a) from the areas of low fluorescence intensity between the strands (amorphous areas) in Figure 11, b) from the center of the strands.

compared with **3b** in different solvents and assembled states. Notably a similar bathochromic shift of the emission maxima has been observed for a perylene bisimide cyclophane by Langhals and co-workers, which they attributed to excitonic coupling in a J-type aggregate.[36] Taken together with the evidence for excitonic interactions given by the changes in the absorption spectra (Figures 9, 10), we conclude that the mesoscopic strands exhibit structural and energetic disorder somewhere in between a crystalline and an amorphous solid state material.

Conclusion

Following examples from nature, self-organization of functional building blocks to extended three-dimensional superstructures might open a new avenue towards light harvesting nanoscopic and mesoscopic assemblies. As a first step in this direction we studied perylene bisimide–melamine assemblies which self-organize hierarchically by means of orthogonal noncovalent interactions as given with hydrogen bonding and π–π interactions as well as the important role of the solvent. The latter was elucidated by systematic binding studies between monotopic receptor compounds **5** and **9** in eight solvents. These studies confirmed that high degrees of complexation based on triple hydrogen bonding between imides and melamines require a noncompetitive environment as realized only in aliphatic solvents. If appropriate substituents are introduced into the supramolecular building blocks for solubilization this approach is an elegant and easy way to increase the binding constant by several orders of magnitude and to enable the formation of supramolecular polymers by triple hydrogen bonding of ditopic perylene bisimides **3** and melamines **8**.

0947-6539/00/0621-3882 $ 17.50+.50/0 *Chem. Eur. J.* **2000**, *6*, No. 21

As our further studies have shown, strong hydrogen bonding is necessary for the formation of a supramolecular polymer chain but is not sufficient for the formation of extended three-dimensional superstructures. Additional intermolecular interactions have to be present to accomplish the formation of extended assemblies already in dilute solution. The rather rigid nature of the triple hydrogen-bonded supramolecular chain of $(\mathbf{3}\cdot\mathbf{8})_n$ makes such an interaction possible by providing an extended aromatic surface prone to $\pi-\pi$ stacking in aliphatic environments. However, from the nine combinations of perylene bismides **3a–c** with melamines **8a–c** only stoichiometric mixtures of *tert*-butylphenoxy substituted perylene bisimide **3b** and long-chain melamines **8b, c** assembled by means of $\pi-\pi$ contacts affording extended three-dimensional superstructures. The other perylene bisimides are either too insoluble (**3a**) or exhibit too bulky substituents (**3c**) to accomplish the demanded second $\pi-\pi$ interaction.

The intact functionality of the perylene chromophores within these superstructures could be demonstrated by bright fluorescence in dilute and concentrated solutions and on surfaces as revealed by confocal optical microscopy. We could show that the fluorescence quantum yield remained almost unity upon hydrogen bond formation between perylene imide dyes **3b, 5** and melamines **8, 9**. On the other hand, $\pi-\pi$ stacking resulted in a reduced fluorescence efficiency in the solid state environment of the mesoscopic strands as is often observed for aggregated dyes.[35] Remaining questions such as the packing arrangement of the molecular building blocks within these assemblies as well as studies on truly supramolecular functionalities, for example light harvesting and long-range vectorial transport of excitation energy within superstructures of nano- and mesoscopic dimensions are topics which we will address in the future.

Experimental Section

Materials and methods: Solvents and reagents were purchased from Merck, Darmstadt (Germany) unless stated otherwise and purified and dried according to standard procedures.[37] *N,N′*-Dibutyl-1,6,7,12-tetraphenoxyperylene-3,4:9,10-tetracarboxylic acid bisimides (**1a–c**) and 1,6,7,12-tetraphenoxyperylene-3,4:9,10-tetracarboxylic acid bisanhydrides (**2a–c**) were synthesized according to the literature.[5, 6] The solvents for binding studies and the preparation of samples for microscopy were of spectroscopic grade and used as received (methylcyclohexane was purchased from Aldrich). Column chromatography was performed on silica gel (Merck silica gel 60, mesh size 0.2–0.5 mm). UV/Vis spectra were taken on a Perkin–Elmer Lambda 40P spectrometer and fluorescence spectra were measured on a SPEX Fluorolog 2 spectrofluorometer. NMR spectra were recorded on a Bruker AC 200 spectrometer using TMS as internal standard.

The melamines **8a–c** were synthesized according to literature procedures.[11, 12]

1,6,7,12-Tetraphenoxyperylene-3,4:9,10-tetracarboxylic acid bisimide (3a): A solution of **2a** (0.19 g, 0.25 mmol) in propionic acid (35 mL) was added dropwise at 120 °C to a solution of ammonium acetate (Fluka, 4.0 g) in propionic acid (30 mL). The resulting dark suspension was stirred at 140 °C for 16 h. After cooling to room temperature, the dark solid was collected on a glass filter funnel and washed neutral with water to give the crude product (0.15 g, 79 %). M.p. > 350 °C. Purification was accomplished by conversion to **4a** (40 %) and subsequent acidic cleavage of the protecting groups by adding a solution of trifluoroacetic acid (2.0 mL) in CH_2Cl_2 (3.0 mL) to a solution of **4a** (47.9 mg, 0.05 mmol) in CH_2Cl_2 (15.0 mL). The dark precipitate was separated by centrifugation to give **3a** (37.0 mg, 98 %); m.p. > 350 °C; FAB-MS: *m/z* (%): 759.2 (100) $[M]^+$; elemental analysis calcd (%) for $C_{48}H_{26}N_2O_8$ (758.8): C 75.98, H 3.45, N 3.69; found C 75.47, H 3.13, N 3.39. Due to its low solubility, no NMR spectra could be recorded for **3a**.

***N,N′*-Di(*tert*-butoxycarbonyl)-1,6,7,12-tetraphenoxyperylene-3,4:9,10-tetracarboxylic acid bisimide (4a)**: A solution of di-*tert*-butyldicarbonate (Boc_2O) (129.8 mg, 0.52 mmol) in dry DMF (1.0 mL) was added at ambient temperature to a suspension of crude **3a** (99.8 mg, 0.13 mmol) in dry DMF (1.0 mL). 4-Dimethylaminopyridine (DMAP) (1.6 mg, 0.013 mmol) was added, and the reaction mixture was stirred under Ar for 4 h. The raw product was precipitated from the resulting red solution by addition of water (4 mL), collected on a glass filter funnel, washed with water, dried, and purified by column chromatography on silica (CH_2Cl_2/*n*-hexane/triethylamine 80:16:4) to yield **4a** (50.3 mg, 40 %); m.p. 80–100 °C (decomp.); ^{1}H NMR (200 MHz, $CDCl_3$, 25 °C, TMS): $\delta = 8.18$ (s, 4H), 7.24 (m, 8H), 7.12 (m, 4H), 6.94 (m, 8H), 1.64 (s, 18H; *t*Bu); UV/Vis (CH_2Cl_2): λ_{max} (ε) = 578 (44600), 539 (28100), 449 (16600), 279 (37200), 265 nm (40900 $mol^{-1}dm^3cm^{-1}$); fluorescence (CH_2Cl_2): $\lambda_{max} = 611$ nm; elemental analysis calcd (%) for $C_{58}H_{42}N_2O_{12}$ (959.0): C 72.64, H 4.41, N 2.92; found C 72.40, H 4.64, N 2.84.

1,6,7,12-Tetra(4-*tert*-butylphenoxy)perylene-3,4:9,10-tetracarboxylic acid bisimide (3b): A solution of **2b** (0.25 g, 0.25 mmol) and ammonium acetate (4.0 g) in propionic acid (30 mL) was stirred at 140 °C for 16 h. After cooling to room temperature, the resulting dark suspension was diluted with water (60 mL). After the reaction mixture was allowed to stand for 3 h, the dark precipitate was collected on a Büchner funnel, washed neutral with water, dried, and purified by column chromatography on silica gel (CH_2Cl_2/MeOH 98:2). The product was isolated from the eluent by precipitation with MeOH (0.15 g, 60 %); m.p. > 350 °C; ^{1}H NMR (200 MHz, $CDCl_3$, 25 °C, TMS): $\delta = 8.43$ (s, 2H; NH), 8.21 (s, 4H), 7.24 (d, $J = 8.7$ Hz, 8H), 6.92 (d, $J = 8.7$ Hz, 8H), 1.30 (s, 36H; *t*Bu); UV/Vis (CH_2Cl_2): λ_{max} (ε) = 580 (40300), 540 (24700), 452 (16700), 293 (37800), 264 nm (42100 $mol^{-1}dm^3cm^{-1}$); fluorescence ($CHCl_3$): $\lambda_{max} = 618$ nm; fluorescence quantum yield $\Phi_f = 95$ %; elemental analysis calcd (%) for $C_{64}H_{58}N_2O_8$ (983.2): C 78.19, H 5.95, N 2.85; found C 77.98, H 6.03, N 2.75. If larger amounts of pure **3b** are desired, a more convenient purification procedure is given by the conversion to Boc-protected dye **4b** and subsequent cleavage as described for **3a**.

***N,N′*-Di(*tert*-butoxycarbonyl)-1,6,7,12-tetra(4-*tert*-butylphenoxy)perylene-3,4:9,10-tetracarboxylic acid bisimide (4b)**: This compound was synthesized as described above for **4a**, starting from crude **3b** (147.4 mg, 0.15 mmol), Boc_2O (148.6 mg, 0.60 mmol), and DMAP (1.8 mg, 0.015 mmol). The product was obtained after chromatography and precipitation with MeOH (74.6 mg, 42 %). M.p. 80–100 °C (decomp.); ^{1}H NMR (200 MHz, $CDCl_3$, 25 °C, TMS): $\delta = 8.21$ (s, 4H), 7.23 (d, $J =$ 9.0 Hz, 8H), 6.82 (d, $J = 9.0$ Hz, 8H), 1.61 (s, 18H; *t*Bu), 1.29 (s, 36H; *t*Bu); UV/Vis (CH_2Cl_2): λ_{max} (ε) = 583 (44700), 544 (27900), 454 (18300), 288 (40300), 266 nm (45500 $mol^{-1}dm^3cm^{-1}$); fluorescence (CH_2Cl_2): $\lambda_{max} =$ 617 nm; elemental analysis calcd (%) for $C_{58}H_{42}N_2O_{12}$ (1183.4): C 75.11, H 6.30, N 2.37; found C 74.93, H 6.41, N 2.29.

1,6,7,12-Tetra(4-(1,1,3,3-tetramethylbutyl)phenoxy)perylene-3,4:9,10-tetracarboxylic acid bisimide (3c): A slow stream of NH_3 was bubbled into a suspension of **2c** (0.36 g, 0.30 mmol) and $Zn(OAc)_2$ (Fluka, 0.25 g) in *N*-methyl-2-pyrrolidone (NMP) (50 mL) at 80 °C for 8 h. After cooling to room temperature, the reaction mixture was stirred slowly into 2 M HCl (150 mL). The precipitate was collected on a Büchner funnel, washed with water, dried, and purified by column chromatography on silica gel (CH_2Cl_2/MeOH 98:2). The product was isolated from the eluent by precipitation with MeOH (0.15 g, 40 %); m.p. 347–350 °C; ^{1}H NMR (200 MHz, $CDCl_3$, 25 °C, TMS): $\delta = 8.32$ (s, 2H; NH), 8.11 (s, 4H), 7.33 (d, $J = 8.4$ Hz, 8H), 6.87 (d, $J = 8.4$ Hz, 8H), 1.73 (s, 8H), 1.37 (s, 24H), 0.78 (s, 36H; *t*Bu); UV/Vis (CH_2Cl_2): λ_{max} (ε) = 581 (40100), 544 (25000), 449 (17200), 290 (39300), 264 nm (44200 $mol^{-1}dm^3cm^{-1}$); fluorescence (CH_2Cl_2): $\lambda_{max} = 614$ nm; elemental analysis calcd (%) for $C_{80}H_{90}N_2O_8$ (1207.6): C 79.57, H 7.51, N 2.32; found C 79.34, H 7.49, N 2.21.

***N*-(2-Ethylhexyl)-1,6,7,12-tetra(4-*tert*-butylphenoxy)perylene-3,4:9,10-tetracarboxylic acid bisimide (5)**: A solution of **2b** (493 mg, 0.50 mmol) and 2-ethylhexylamine (82 μL, 0.50 mmol) in toluene (30 mL) was refluxed for 20 h. The solvent was evaporated and propionic acid (30 mL) was added to

the residue. A slow stream of ammonia was bubbled into the reaction mixture until its weight was increased by 1.9 g. The reaction mixture was then refluxed for another 14 h. After cooling to room temperature, the crude product was precipitated from the red solution by addition of water (60 mL), washed neutral with water, and dried. Separation of **5** from the symmetrically substituted by-products was achieved by column chromatography on silica gel (CH_2Cl_2) to yield pure **5** (140.3 mg, 26 %); m.p. 315–320 °C (subl.); ^{1}H NMR (200 MHz, $CDCl_3$, 25 °C, TMS): $\delta = 8.44$ (s, 1H; NH), 8.23 (s, 2H), 8.22 (s, 2H), 7.23 (d, $J = 8.7$ Hz, 8H), 6.82 (d, $J = 8.7$ Hz, 8H), 4.04 (m, 2H), 1.86 (m, 1H), 1.4–1.2 (m, 8H), 1.29 (s, 36H; *t*Bu), 0.89 (m, 6H); UV/Vis (CH_2Cl_2): λ_{max} (ε) = 579 (44800), 539 (27700), 451 (17800), 288 (45400), 265 nm (43000 $mol^{-1} dm^3 cm^{-1}$); fluorescence (CH_2Cl_2): $\lambda_{max} = 614$ nm; elemental analysis calcd (%) for $C_{72}H_{74}N_2O_8$ (1095.4): C 78.95, H 6.81, N 2.56; found C 78.69, H 6.92, N 2.41.

***N,N′*-Di(2-ethylhexyl)-1,6,7,12-tetra(4-*tert*-butylphenoxy)perylene-3,4:9,10-tetracarboxylic acid bisimide** (**6**): A suspension of **2b** (0.20 g, 0.2 mmol) and 2-ethylhexylamine (0.26 mL, 1.6 mmol) in propionic acid (5.0 mL) was stirred for 10 h at 140 °C. After cooling to room temperature, the red precipitate was collected on a Büchner funnel and washed with methanol (0.20 g, 83 %); m.p. 304 °C; ^{1}H NMR (200 MHz, $CDCl_3$, 25 °C, TMS): $\delta =$ 8.24 (s, 4H), 7.23 (d, $J = 8.9$ Hz, 8H), 6.83 (d, $J = 8.9$ Hz, 8H), 4.04 (m, 4H), 1.87 (m, 2H), 1.4–1.2 (m, 16H), 1.29 (s, 36H; *t*Bu), 0.89 (m, 12H); UV/Vis (CH_2Cl_2): λ_{max} (ε) = 578 (46500), 539 (29000), 451 (17900), 287 (53300), 266 nm (42900 $mol^{-1} dm^3 cm^{-1}$); fluorescence (CH_2Cl_2): $\lambda_{max} = 610$ nm; elemental analysis calcd (%) for $C_{80}H_{90}N_2O_8$ (1207.6): C 79.57, H 7.51, N 2.32; found C 79.48, H 7.50, N 2.31.

2,4-Diamino-6-di(2-ethylhexyl)amino-1,3,5-triazine (**9**): A suspension of 2-chloro-4,6-diamino-1,3,5-triazine[38] (1.46 g, 10 mmol), di(2-ethylhexyl)-amine (Fluka, 3.31 mL, 11 mmol) and $NaHCO_3$ (0.93 g, 11 mmol) in dry DMF (50 mL) was stirred under Ar at 140 °C for 24 h. After cooling to room temperature, the mixture was poured into water (200 mL). The resulting emulsion was extracted with CH_2Cl_2 (3 × 50 mL). The combined extracts were dried over NaCl, and concentrated to yield a yellow oil (4 g). Column chromatography on silica gel (ethyl acetate) yielded a colorless oil (2.9 g) which crystallized slowly at 4 °C. The solid was washed with cold *n*-pentane to yield colorless tiny crystals (2.02 g, 58 %). M.p. 60 °C; ^{1}H NMR (200 MHz, $CDCl_3$, 25 °C, TMS): $\delta = 4.78$ (s, 4H; NH), 3.41 (d, $J = 7.3$ Hz, 4H), 1.75 (m, 2H), 1.4–1.1 (m, 16H), 0.87 (m, 12H); elemental analysis calcd (%) for $C_{19}H_{38}N_6$ (350.6): C 65.10, H 10.93, N 23.97; found C 65.02, H 10.73, N 23.77.

NMR titration experiments: NMR titrations were performed at 7×10^{-3} mol L^{-1} constant perylene imide receptor concentration (7×10^{-3} mol L^{-1} for **5**, 3.5×10^{-3} mol L^{-1} for **3b**) at a temperature of 298 K. Aliquots of a guest solution (melamine receptor concentration 3.5×10^{-2} mol L^{-1}, containing 7×10^{-3} mol L^{-1} host receptor concentration) were subsequently added to a NMR tube containing an initial volume of 350 μL host solution. After each addition, a spectrum was recorded. In all investigated solvents, a sufficiently sharp peak was obtained for the imide proton throughout the experiment. The association constants were determined by nonlinear least-squares regression analysis from the change in chemical shift of the imide proton.[39]

UV/Vis titration experiments: Titrations were performed at 2.5×10^{-5} mol L^{-1} constant host concentration at room temperature. Two 1 cm quartz cuvettes with 1500 μL host solution and 1500 μL pure solvent were placed in a double beam spectrophotometer. Guest solutions of 2.5×10^{-4} mol L^{-1} were prepared in host solution and in pure solvent. Aliquots of these solutions were added to the cuvette with the host solution and in the reference cuvette, respectively, and a spectrum was recorded after every addition. The association constants were determined by nonlinear least-squares regression analysis from the absorbance change at several wavelengths.[39]

Fluorescence measurements: Fluorescence measurements were done with a calibrated SPEX Fluorolog 2 spectrofluorometer, and all spectra were corrected.

The fluorescence quantum yields were determined by the optically dilute method[40] using *N,N′*-di(2,6-diisopropylphenyl)-1,6,7,12-tetraphenoxyperylene-3,4:9,10-tetracarboxylic acid bisimide as reference ($\Phi_{f,CHCl_3} =$ 0.96).[5a, 24] The refractive indices of the solvents used in the quantum yield calculations were obtained from the CRC handbook.[41] The given quantum yields were averaged from values at three excitation wavelengths in the range from 560–590 nm with a standard deviation $\sigma = 2$–3 %. All solutions were prepared from air-saturated solvents. For comparison, the reference perylene dye was also studied after degasing (six freeze drying cycles at ultra-high vacuum) to make sure that the influence of oxygen is indeed negligible for the given chromophoric system.

Fluorescence titration studies: Titrations were performed at 1×10^{-6} mol L^{-1} constant host concentration at room temperature. At the low chromophore concentration which is demanded to rule out quenching by reabsorption, a large excess of melamine was needed to obtain a measurable effect. Thus a guest solution of 1×10^{-4} mol L^{-1} was prepared in host solution and added in small aliquots to the cell with the host solution (initial volume 1500 μL). Spectra with excitation wavelengths of 530 and 570 nm were recorded after each addition. The association constants were determined by nonlinear least-squares regression analysis from the fluorescence intensity change at different wavelengths as well as the integrated fluorescence intensity.[39]

Fluorescence spectroscopy of concentrated solutions: Owing to the high optical densities of the solutions required for aggregate formation, these measurements were not performed using the conventional right angle setup, but the front face illumination technique on a 1 mm cell. In order to estimate the quantum yield of the assemblies **3b·8c**, a calibration curve was established for the non-aggregating perylene bisimide dye **6** ($\Phi_{f,MCH} =$ 0.96) in methylcyclohexane at the same concentrations and under the same experimental conditions. For this compound, the emission fine structure and peak position remained unchanged, but for the higher concentrations, the observed fluorescence intensity showed a nonlinear dependence on the concentration. This deviation from linearity could be fully described by Equation (3), which results from the application of Beer's law to the excitation light in the sample.[42]

$$I_f = \Phi_f I_0 (1 - e^{-2.303\varepsilon(\lambda)cd}) \quad (3)$$

In Equation (3), I_f is the observed fluorescence intensity, Φ_f is the fluorescence quantum yield, I_0 is the intensity of the excitation beam, $\varepsilon(\lambda)$ is the molar extinction coefficient of the sample at the excitation wavelength, c is the concentration of the sample, and d is the optical path length. The concentration-dependent fluorescence intensities for **6** could be fitted in excellent agreement to Equation (3), which suggests again that **6** shows no aggregation, and more importantly, that reabsorption can be neglected in this range of concentration and under these experimental conditions. Moreover, the value of $d = 0.83$ mm which was obtained for the optical path length from nonlinear regression using Equation (3) is in good agreement with the cell dimension of 1 mm and suggests that the major contribution to the fluorescence signal originates from the bulk of the sample and not from a thin layer at the surface. Therefore, the described experimental setup was suitable for the investigation of methylcyclohexane solutions of the aggregated system **3b·8c**, which showed more pronounced changes in the fluorescence intensity for increasing concentrations (Figure 9d). By comparing the fluorescence intensities observed for **3b·8c** to those of **6** at the same concentrations, also for the former quantitative fluorescence data could be obtained.

Preparation of perylene bisimide – melamine complexes: Equal amounts of 10^{-3} mol L^{-1} stock solutions of perylene bisimides **3b, c** ($CHCl_3$) and melamines **8b, c** ($CHCl_3$/methylcyclohexane 1:1) were combined in a flask, and the solvent was evaporated under reduced pressure. The resulting violet film was dissolved in methylcyclohexane by sonication for 2 min and again the solvent was evaporated. This procedure was repeated at least twice to ensure complete removal of chloroform. The dispersions obtained were stable for at least seven days (**3b·8b**) and three months (**3b·8c**).

Dynamic light scattering: Dynamic light scattering (DLS) has been used to determine the hydrodynamic radius R of **3b·8c** assemblies at a concentration of 5×10^{-5} mol L^{-1} in methylcyclohexane. The experimental setup consisted of a Kr^+ laser, operating at wavelength $\lambda = 647.1$ nm and laser power attenuated to 50 mW to avoid local heating of the sample by light absorption, a homebuilt goniometer to adjust the scattering angle, and a pinhole detector to measure the scattered intensity as a function of time. Intensity time correlation functions have been obtained from the scattered intensity using an ALV 3000 hardware correlator. All samples have been purified from dust by filtration with Millipore filters, pore size 0.5 μm, and put into cylindrical Suprasil light scattering cuvettes of diameter 10 mm. It

0947-6539/00/0621-3884 $ 17.50+.50/0 *Chem. Eur. J.* **2000**, *6*, No. 21

should be noted that at the beginning, the dye aggregates adsorbed at the filter to give a nearly colorless filtrate. Therefore, the first 2–3 mL of solution were discarded before the sample used for light scattering experiments was collected. By comparing the absorbance of the filtrate and the initial solution, we could verify that during this procedure no change in the concentration had occured. During the measurement, the samples have been placed in a toluene bath of constant temperature to avoid diffraction from the glass walls of the cuvettes, and to keep the sample temperature constant at $T = 20\,^{\circ}\mathrm{C}$.

Intensity time correlation functions $G_2(q,t)$ have been fitted to a stretched-exponential decay function according to Equation (4):

$$G_2(q,t) = (A \exp(-(t/\tau)^{\beta}))^2 \tag{4}$$

A is the signal amplitude, t the correlation time, τ the characteristic relaxation time, and β the so-called stretching parameter which provides a measure for the polydispersity of the sample. For monodisperse spherical systems, β should be 1.0. For polydisperse systems, β is well below 1.0, that is typically 0.7–0.9. Here, it should be noted that β provides a quantitative measure for the standard deviation of the particle size distribution in case a characteristic distribution function, for example Gaussian, is assumed. The average relaxation time $\langle\tau\rangle$ is calculated according to:

$$\langle\tau\rangle = \frac{\Gamma(\beta^{-1})}{\beta} \tag{5}$$

where Γ is the Gamma function. From $\langle\tau\rangle$ and the scattering vector q, the apparent translational diffusion coefficient $D_{\mathrm{app}}(q)$ is calculated:

$$D_{\mathrm{app}}(q) = (\langle\tau\rangle q^2)^{-1} \tag{6a}$$

and

$$q = \frac{4\pi n \sin(\theta/2)}{\lambda} \tag{6b}$$

with the refractive index n of the solvent, the scattering angle θ and the laser wavelength λ. Finally, the hydrodynamic radius $R_{\mathrm{app}}(q)$ of the scattering particles is calculated by the Stokes–Einstein equation:

$$R_{\mathrm{app}}(q) = \frac{kT}{6\pi\eta\, D_{\mathrm{app}}(q)} \tag{7}$$

where η is the viscosity of the solvent. For monodisperse rigid particles, $R_{\mathrm{app}}(q) = R$ is independent of the scattering vector q. For polydisperse systems, however, the signal at smaller scattering vectors is more dominated by the particle fraction of larger size, leading to an increase of the apparent particle size $R_{\mathrm{app}}(q)$ with decreasing q. An additional complication occurs in case of non-rigid flexible particles or rod-like systems: in these cases, intramolecular structure fluctuations and/or rotational motions of the scattering particles especially at larger q, that is at shorter length scales, contribute to the correlation function and lead to a decrease of the apparent particle size with increasing q. For these reasons, such systems are best characterized by interpolating $D_{\mathrm{app}}(q)$ or $R_{\mathrm{app}}(q)^{-1}$ to $q = 0$, that is infinite experimental length scale, where all scattering particles should contribute to the signal according to their size and concentration, and the correlation function is dominated by translational diffusion. The resulting size R_{app} $(q = 0) = R$ therefore corresponds to an inverse z-average, namely:

$$R^{-1} = \frac{\sum n_i M_i^2 R_i^{-1}}{\sum n_i M_i^2} \tag{8}$$

where M_i is the molecular weight of scattering particles of size R_i, and n_i their number density.

Electron microscopy: For transmission electron microscopy, a drop of a $5 \times 10^{-5}\,\mathrm{mol\,L^{-1}}$ solution of the perylene bisimide–melamine complexes in methylcyclohexane was evaporated on a formvar/carbon coated nickel grid (200 mesh). Staining was either achieved by placing the sample on a drop of concentrated aqueous uranyl acetate solution for 15 min and subsequently rinsing the sample with water or by exposing the specimen to a saturated atmosphere of osmium tetroxide vapor for 2 h. The specimens were examined in a Zeiss EM 10 transmission electron microscope operating at 80 kV.

For scanning electron microscopy, the TEM grids were sputtered with a chromium layer (5 nm) and examined in a Zeiss DSM 920 scanning electron microscope.

Confocal fluorescence microscopy and spatially resolved fluorescence spectroscopy: A drop of the perylene bisimide–melamine solution was evaporated on a glass slide which was previously treated with freshly distilled trimethylchlorosilane for 12 h and rinsed twice with methanol. The specimens were examined with a WITec α-SNOM in the confocal fluorescence mode. For excitation, a He/Ne laser was used ($\lambda = 543$ nm, $P = 40$ μW). By using a RG 590 fluorescence filter, only wavelengths above 590 nm were detected. Spatially resolved fluorescence spectra were measured with a SpectraPro-300i spectrometer (Acton Research Corp.), which was linked to the confocal microscope by an optical fiber. A 20 μm × 20 μm area of the sample was scanned (128 × 128 pixel), and a spectrum was recorded for each pixel.

Acknowledgements

This work was supported by the Deutsche Forschungsgemeinschaft (scholarship for C.T. within Graduiertenkolleg 328 "Molecular Organization and Dynamics at Interfaces and Surfaces"), the Ulmer Universitätsgesellschaft, the Fonds der Chemischen Industrie and the BMBF (Liebig grant for F.W.) and BASF AG. We are indebted to Prof. Paul Walther for the possibility to carry out electron microscopy in the Sektion Elektronenmikroskopie and to Prof. Peter Bäuerle (Abt. Organische Chemie II) for his support.

[1] Review articles on superstructure formation in chemistry: a) H. Ringsdorf, B. Schlarb, J. Venzmer, *Angew. Chem.* **1988**, *100*, 117–162; *Angew. Chem. Int. Ed. Engl.* **1988**, *27*, 113–158; b) M. Antonietti, C. Göltner, *Angew. Chem.* **1997**, *109*, 944–964; *Angew. Chem. Int. Ed.* **1997**, *36*, 910–928; c) J.-H. Fuhrhop in *Comprehensive Supramolecular Chemistry*, *Vol. 9* (Eds.: J. L. Atwood, J. E. D. Davies, D. D. MacNicol, F. Vögtle), Pergamon, Oxford, **1996**, pp. 407–450; d) J.-M. Lehn, *Supramolecular Chemistry*, VCH, Weinheim, **1995**; e) F. Vögtle, *Supramolekulare Chemie*, Teubner, Stuttgart, **1989**; f) D. S. Lawrence, T. Jiang, M. Levett, *Chem. Rev.* **1995**, *95*, 2229–2260; g) D. Philp, J. F. Stoddart, *Angew. Chem.* **1996**, *108*, 1242–1286; *Angew. Chem. Int. Ed.* **1996**, *35*, 1154–1196.

[2] a) G. McDermott, S. M. Prince, A. A. Freer, A. M. Hawthornthwaite-Lawless, M. Z. Papiz, R. J. Cogdell, N. W. Isaacs, *Nature* **1995**, *374*, 517–521; b) X. Hu, K. Schulten, *Physics Today* **1997**, *50(8)*, 28–38; c) T. Pullerits, V. Sundström, *Acc. Chem. Res.* **1996**, *29*, 381–389.

[3] a) A. P. H. J. Schenning, F. B. G. Benneker, H. P. M. Geurts, X. Y. Liu, R. J. M. Nolte, *J. Am. Chem. Soc.* **1996**, *118*, 8549–8552; b) C. F. van Nostrum, *Adv. Mater.* **1996**, *8*, 1027–1030; c) H. Engelkamp, S. Middelbeek, R. J. M. Nolte, *Science* **1999**, *284*, 785–788.

[4] a) E. E. Simanek, X. Li, I. S. Choi, G. M. Whitesides in *Comprehensive Supramolecular Chemistry*, *Vol. 9* (Eds.: J. L. Atwood, J. E. D. Davies, D. D. MacNicol, F. Vögtle), Pergamon, Oxford, **1996**, pp. 595–621; b) C. Fouquey, J.-M. Lehn, A.-M. Levelut, *Adv. Mater.* **1990**, *2*, 254–257; c) T. Gulik-Krzywicki, C. Fouquey, J.-M. Lehn, *Proc. Natl. Acad. Sci. USA* **1993**, *90*, 163–167; d) N. Kimizuka, T. Kawasaki, K. Hirata, T. Kunitake, *J. Am. Chem. Soc.* **1995**, *117*, 6360–6361; e) N. Kimizuka, S. Fujikawa, H. Kuwahara, T. Kunitake, A. Marsh, J.-M. Lehn, *J. Chem. Soc. Chem. Commun.* **1995**, 2103–2104; f) K. Ariga, T. Kunitake, *Acc. Chem. Res.* **1998**, *31*, 371–378; g) R. F. M. Lange, F. H. Beijer, R. P. Sijbesma, R. W. W. Hooft, H. Kooijman, A. L. Spek, J. Kron, E. W. Meijer, *Angew. Chem.* **1997**, *109*, 1006–1008; *Angew. Chem. Int. Ed.* **1997**, *36*, 969–971; h) T. M. Bohanon, S. Denzinger, R. Fink, W. Paulus, H. Ringsdorf, M. Weck, *Angew. Chem.* **1995**, *107*, 102–104; *Angew. Chem. Int. Ed.* **1995**, *34*, 58–60; i) W.Yang, S. Chen, X. Chai, Y. Cao, R. Lu, W. Chai, Y. Jiang, T. Li, J.-M. Lehn, *Synth. Met.* **1995**, *71*, 2107–2108; j) W. Yang, X. Chai, L. Chi, X. Liu, Y. Cao, R. Lu, Y. Jiang, X. Tang, H. Fuchs, T. Li, *Chem. Eur. J.* **1999**, *5*, 1144–1149; k) K. A. Jolliffe, P. Timmerman, D. N. Reinhoudt, *Angew. Chem.* **1999**, *111*, 983–986; *Angew. Chem. Int. Ed.* **1999**, *38*, 933–937; l) H.-A. Klok, K. A. Jolliffe, C. L. Schauer,

L. J. Prins, J. P. Spatz, M. Möller, P. Timmerman, D. N. Reinhoudt, *J. Am. Chem. Soc.* **1999**, *121*, 7154 – 7155.
[5] a) G. Seybold, G. Wagenblast, *Dyes Pigm.* **1989**, *11*, 303 – 317; b) D. Dotcheva, M. Klapper, K. Müllen, *Macromol. Chem. Phys.* **1994**, *195*, 1905 – 1911; c) H. Quante, P. Schlichting, U. Rohr, Y. Geerts, K. Müllen, *Macromol. Chem. Phys.* **1996**, *197*, 4029 – 4044; d) U. Rohr, P. Schlichting, A. Böhm, M. Groß, K. Meerholz, C. Bräuchle, K. Müllen, *Angew. Chem.* **1998**, *110*, 1463 – 1467; *Angew. Chem. Int. Ed.* **1998**, *37*, 1434 – 1437.
[6] A part of this work appeared in a short communication: F. Würthner, C. Thalacker, A. Sautter, *Adv. Mater.* **1999**, *11*, 754 – 758.
[7] a) H. Zollinger, *Color Chemistry*, 2nd ed., VCH, Weinheim, **1991**; b) W. Herbst, K. Hunger, *Industrial Organic Pigments*, *Production*, *Properties*, *Applications*, WILEY-VCH, Weinheim, **1997**.
[8] a) H. Langhals, *Heterocycles* **1995**, *40*, 477 – 500, and references therein; b) H. Kaiser, J. Lindner, H. Langhals, *Chem. Ber.* **1991**, *124*, 529 – 535.
[9] J. S. Zambounis, Z. Hao, A. Iqbal, *Nature* **1997**, *388*, 131 – 132.
[10] H. M. Deutsch, L. T. Gelbaum, M. McLaughlin, T. J. Fleischmann, L. L. Earnhart, R. D. Haugwitz, L. H. Zalkow, *J. Med. Chem.* **1986**, *29*, 2164 – 2170.
[11] T. Irikura, Y. Abe, K. Okamura, K. Higo, A. Maeda, F. Morinaga, G. Shirai, S. Hatae, *J. Med. Chem.* **1970**, *13*, 1081 – 1089.
[12] a) H. Koyano, P. Bissel, K. Yoshihara, K. Ariga, T. Kunitake, *Chem. Eur. J.* **1997**, *3*, 1077 – 1082; b) K. Ariga, A. Kamino, H. Koyano, T. Kunitake, *J. Mater. Chem.* **1997**, *7*, 1155 – 1161.
[13] a) M. Mammen, E. E. Simanek, G. M. Whitesides, *J. Am. Chem. Soc.* **1996**, *118*, 12614 – 12623; b) F. H. Beijer, R. P. Sijbesma, H. Kooijman, A. L. Spek, E. W. Meijer, *J. Am. Chem. Soc.* **1998**, *120*, 6761 – 6769.
[14] a) K. A. Connors, *Binding Constants*, Wiley, New York, **1987**; b) C. S. Wilcox in *Frontiers of Supramolecular Chemistry and Photochemistry* (Eds.: H. J. Schneider, H. Dürr), VCH, Weinheim, **1991**, pp. 123 – 143.
[15] a) F. Würthner, J. Rebek, Jr., *J. Chem. Soc. Perkin Trans. 2* **1995**, 1727 – 1734; b) H. L. Anderson, C. A. Hunter, M. N. Meah, J. K. M. Sanders, *J. Am. Chem. Soc.* **1990**, *112*, 5780 – 5789; c) P. N. Taylor, H. L. Anderson, *J. Am. Chem. Soc.* **1999**, *121*, 11538 – 11545.
[16] A. P. Bisson, C. A. Hunter, J. C. Morales, K. Young, *Chem. Eur. J.* **1998**, *4*, 845 – 851.
[17] Hydrogen-bond formation between the imide NH and the nitrogen lone pair of the melamine should be less important because of nodes of the HOMO and LUMO orbitals at the imide nitrogen, see a) H. Langhals, S. Demmig, H. Huber, *Spectrochim. Acta* **1988**, *44A*, 1189 – 1193; b) S. K. Lee, Y. Zu, A. Herrmann, Y. Geerts, K. Müllen, A. J. Bard, *J. Am. Chem. Soc.* **1999**, *121*, 3513 – 3520.
[18] R. P. Sijbesma, F. H. Beijer, L. Brunsveld, B. J. B. Folmer, J. H. K. K. Hirschberg, R. F. M. Lange, J. K. L. Lowe, E. W. Meijer, *Science* **1997**, *278*, 1601 – 1604.
[19] The formation of 2:1 complexes is described by two association constants K_1 and K_2 which are related by the expression $4K_2 = \alpha K_1$, where α, the interaction parameter, is a measure of the cooperativity between the two ends of the ligand. In the given case, nonlinear regression analysis gave $\alpha \approx 1$, thus indicating two noncooperative binding events. Because the statistical factor of four takes into account the degeneracy of the monobound species, this analysis proves identical enthalpic contributions for both binding events, see also refs. [14, 15].
[20] A study on rotational barriers in trisubstituted triazines can be found in a) A. R. Katritzky, D. C. Oniciu, I. Ghiviriga, R. A. Barcock, *J. Chem. Soc. Perkin Trans. 2* **1995**, 785 – 792; b) A. R. Katritzky, I. Ghiviriga, P. J. Steel, D. C. Oniciu, *J. Chem. Soc. Perkin Trans. 2* **1996**, 443 – 447.
[21] P. J. Flory, *Principles of Polymer Chemistry*, Cornell University Press, Ithaca, **1953**, pp. 317 – 334.
[22] N. Yamaguchi, D. S. Nagvekar, H. W. Gibson, *Angew. Chem.* **1998**, *110*, 2518 – 2520; *Angew. Chem. Int. Ed.* **1998**, *37*, 2361 – 2364.
[23] R. K. Castellano, C. Nuckolls, S. H. Eichhorn, M. R. Wood, A. J. Lovinger, J. Rebek, Jr., *Angew. Chem.* **1999**, *111*, 2764 – 2768; *Angew. Chem. Int. Ed.* **1999**, *38*, 2603 – 2606.
[24] R. Gvishi, R. Reisfeld, Z. Burshtein, *Chem. Phys. Lett.* **1993**, *213*, 338 – 344.
[25] V. Bulović, P. E. Burrows, J. A. Cronin, M. E. Thompson, *Chem. Phys.* **1996**, *210*, 1 – 12.
[26] M. A. Biasutti, S. De Feyter, S. De Backer, G. B. Dutt, F. C. De Schryver, M. Ameloot, P. Schlichting, K. Müllen, *Chem. Phys. Lett.* **1996**, *248*, 13 – 19.
[27] A recent crystal structure of a related dye revealed a torsion angle of 25° for the central ring which agrees favorably with AM1 calculations: F. Würthner, A. Sautter, C. Thalacker, *Angew. Chem.* **2000**, *112*, 1298 – 1301; *Angew. Chem. Int. Ed.* **2000**, *39*, 1243 – 1245.
[28] M. Petersheim, D. H. Turner, *Biochemistry* **1983**, *22*, 256 – 263.
[29] In principle, thermodynamic parameters ΔH and ΔS are accessible from this analysis. However, because of the rather arbitrary choice of the model no values will be given in this paper.
[30] R. Pecora, *Dynamic Light Scattering*, Plenum Press, New York, **1985**.
[31] Preliminary DLS experiments of 5×10^{-5} mol L^{-1} solutions of pure dialkylmelamine **8c** in methylcyclohexane suggest that already in the absence of bisimide dyes large-sized colloidal particles are formed.
[32] A structurally related system where the solvent used for the staining procedure had a substantial effect on superstructure formation is described in ref. [4j].
[33] A rod-like helical structure has been suggested for a melamine-naphthalene bisimide system. See ref. [4d].
[34] a) J. R. Lakowicz, *Principles of Fluorescence Spectroscopy*, 2nd ed., Kluwer Academic/Plenum, New York, **1999**, pp. 516 – 518; b) T. Förster, *Z. Elektrochem.* **1950**, *54*, 42 – 46.
[35] H. Bässler in *Electronic Materials*: *The Oligomer Approach* (Eds.: K. Müllen, G. Wegner), WILEY-VCH, Weinheim, **1998**, pp. 403 – 431.
[36] H. Langhals, R. Ismael, *Eur. J. Org. Chem.* **1998**, 1915 – 1917.
[37] D. D. Perrin, W. L. F. Armarego, *Purification of Laboratory Chemicals*, 2nd ed., Pergamon Press, Oxford, **1980**.
[38] J. T. Thurston, J. R. Dudley, D. W. Kaiser, I. Hechenbleikner, F. C. Schaefer, D. Holm-Hansen, *J. Am. Chem. Soc.* **1951**, *73*, 2981 – 2983.
[39] Systat 5.03, Systat Inc., Evanston, **1990 – 1993**.
[40] J. R. Lakowicz, *Principles of Fluorescence Spectroscopy*, 2nd ed., Kluwer Academic/Plenum, New York, **1999**, pp. 52 – 53.
[41] *CRC Handbook of Chemistry and Physics* (Ed.: D. R. Lide), 72nd ed., CRC Press, Boca Raton, **1991**.
[42] W. Schmidt, *Optische Spektroskopie*, VCH, Weinheim, **1994**, pp. 205 – 207.

Received: March 21, 2000 [F2378]

  0947-6539/00/0621-3886 $ 17.50+.50/0